from genetically engineered animals is still scarce, and *in vivo* validation of such findings is still much awaited. Furthermore, despite the heavy expression of all CaMKI isoforms in the developing forebrain, there is yet little information as to what kinds of endogenous activity or extracellular ligands may influence the activity of CaMKI, during a perinatal period when only spontaneous Ca^{2+} transients are generated, and when synaptic activity-driven Ca^{2+}-mobilization is still missing.

We previously reported that a dendritic raft-anchored CaMK, CaMKIγ/CL3, plays an essential role in dendritic growth downstream of BDNF (Takemoto-Kimura et al., 2007). However, the exact context in which other CaMKI isoforms might contribute to neuronal morphogenesis remained obscure.

Here, we show genetic and pharmacogenetic evidence that demonstrates that two separate limbs of CaMKK–CaMKI cascades, CaMKK–CaMKIα and CaMKK–CaMKIγ, critically coordinate axonal and dendritic morphogenesis of immature cortical neurons, respectively. Furthermore, we found that activation of $GABA_A$ receptors promoted axonal growth via the CaMKK–CaMKIα pathway. During perinatal brain development, *in vivo* knockdown of CaMKIα significantly impaired the terminal elongation of callosal axon projections in the somatosensory cortex. Together, our data suggest that a GABA-driven CaMK cascade may play a critical role in activity-regulated refinement of cortical axon wiring.

Materials and Methods

Construction of expression plasmids and RNA interference vectors. For RNA interference (RNAi) experiments, short hairpin RNA (shRNA) vectors, coexpressing mRFP1 as a morphological tracer, were constructed essentially as described previously (Takemoto-Kimura et al., 2007). To create pSUPER-shCaMKIα and pSUPER-shCaMKIα#2, two complementary 60 bp oligonucleotides carrying sense and antisense sequences for CATTGTAGCCCTGGATGAC (19 bp; corresponding to nucleotides 231-249 of mouse CaMKIα) and antisense and sense sequences for GATCAAGCACCCCAACATT (19 bp; corresponding to nucleotides 216-234 of mouse CaMKIα), respectively, were subcloned into the pSuper+mRFP1 plasmid backbone. pSUPER-shNega was generated similarly except that an artificial 19-mer sequence (ATCCGCGCGATAGTACGTA) was used as a target as described previously (Takemoto-Kimura et al., 2007). This sequence was based on a commercially available negative control small interfering RNA sequence (B-Bridge International), and we confirmed that it had no significant identity to any known mammalian gene based on a BLAST (basic local alignment search tool) search. Silent mutations were introduced into the shRNA target sequence of enhanced green fluorescent protein (EGFP)-tagged wild-type (WT) and mutant CaMKIα cDNAs to generate shRNA-resistant constructs (pEGFP-CaMKIα_{res} and related constructs). Short hairpin RNA interference vectors against CaMKIα, CaMKIγ/CL3, and CaMKIV [shCaMKIα (this study); shCaMKIγ/CL3 and shCaMKIV (Takemoto-Kimura et al., 2007)] selectively suppressed expression of GFP-CaMKIα, GFP-CaMKIγ/CL3, GFP-CaMKIV, respectively (supplemental Fig. 2*A*,*B*, available at www.jneurosci.org as supplemental material). An antibody against CaMKIV (BD Biosciences Transduction Laboratories) also confirmed these results. The potency of the knockdown was estimated to be ~70–80%, based on the reduction of overexpressed GFP-tagged proteins in Western blot analyses (supplemental Fig. 2*B*, available at www.jneurosci.org as supplemental material). In keeping with this, and consistent with a transfection efficiency of >50% in our electroporation, we also detected a target-specific decrease of 40~50% in the amount of endogenous mRNA using a real-time PCR system (LightCycler 1.5; Roche Diagnostics) (supplemental Fig. 2*C*, available at www.jneurosci.org as supplemental material).

Rat CaMKIα cDNA was inserted into pEGFPC1 vector (Clontech) to generate pEGFP-CaMKIα (Takemoto-Kimura et al., 2003). The expression vector for a constitutively active form, pEGFP-CaMKIαCA (286IHQS to 286EDDD; F307A) was created from pEGFP-CaMKIα by

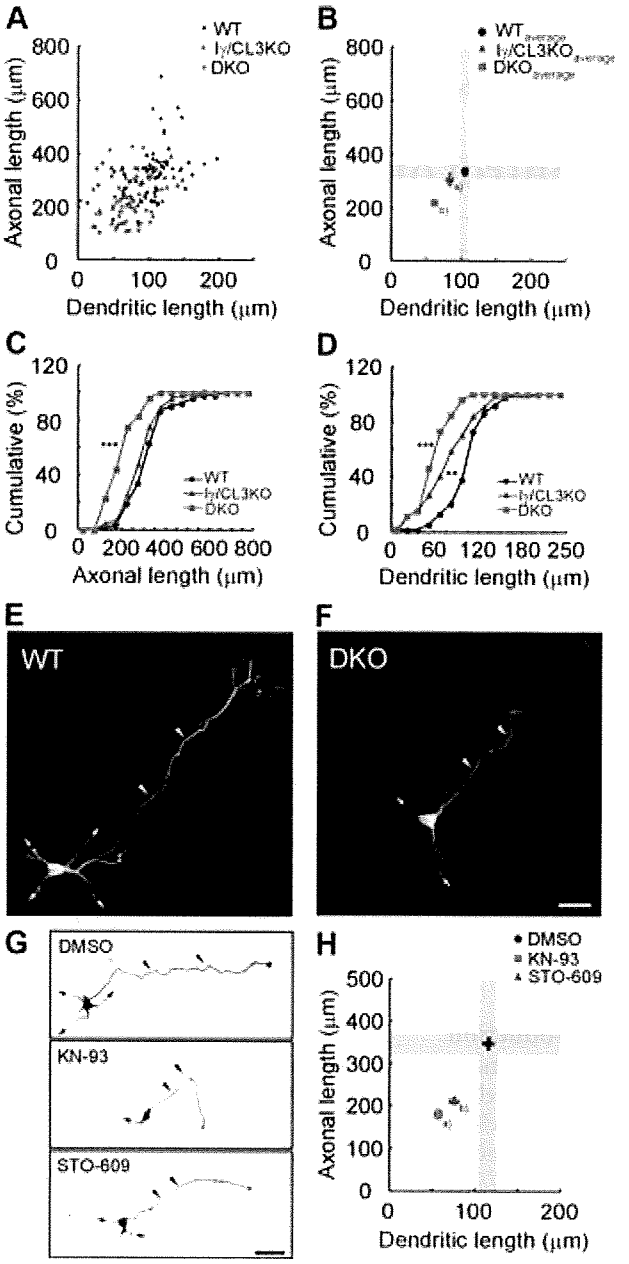

Figure 1. CaMKK-dependent CaMK cascades control cortical axonal and dendritic growth. ***A***, ***B***, A scattered plot (orthogonal plot) of data points (***A***) and averages (***B***) for both axonal and dendritic lengths obtained of individual neurons. Black circles, Wild type (WT). Blue triangles, Iγ/CL3 knock-out (Iγ/CL3 KO). Red squares, CaMKKα/β-double knock-out (DKO). Number of neurons: WT, $n = 52$; Iγ/CL3 KO, $n = 44$; DKO, $n = 52$. [a]Dendrite, $p < 0.01$; [b]Axon, $p < 0.001$; dendrite, $p < 0.001$ (one-way ANOVA with Tukey's test comparison with WT). ***C***, ***D***, Cumulative probability analysis for total axonal length (***C***) and total dendritic length (***D***) in neurons from WT, DKO, and Iγ/CL3 KO mice. Number of neurons: WT, $n = 52$; DKO, $n = 52$; Iγ/CL3 KO, $n = 44$. $^{**}p < 0.01$; $^{***}p < 0.001$, Kolmogorov–Smirnov test comparison with WT. ***E***, ***F***, Cortical neurons (2 d *in vitro*) from CaMKKα/β-DKO mice (***F***) showed impaired growth of axons (arrowheads) and dendrites (arrows) compared with neurons from WT mice (***E***). Scale bar, 25 μm. ***G***, Treatment with KN-93, a general CaMK inhibitor, and STO-609, a blocker of CaMKKα/β, the upstream kinases of all CaMKI/IV, from 6 to 48 h after plating impaired both axonal (arrowheads) and dendritic (arrows) growth. Scale bar, 50 μm. ***H***, An orthogonal plot shows a quantitative analysis of axonal and dendritic morphometric parameters from each neuron. Number of neurons: DMSO, $n = 48$; KN-93, $n = 43$; STO-609, $n = 48$. [a,b]Axon, $p < 0.001$; dendrite, $p < 0.001$ (one-way ANOVA with Tukey's test comparison with DMSO).

site-directed mutagenesis. Similarly, a point mutation was introduced to generate pEGFP-CaMKIαK49A. pCAG-EGFP-CaMKIγ/CL3 was as described previously (Takemoto-Kimura et al., 2007). CaMKKβ wild-type and V269F cDNA (Tokumitsu et al., 2003) (a kind gift from Dr. Hiroshi Tokumitsu, Kagawa University, Kagawa, Japan) was subcloned into pEGFPC3. Mouse CaMKIβ and CaMKIδ cDNAs were obtained from the German RZPD gene collection and RIKEN Genomic Science Center, respectively, and inserted into pEGFPC1 vector to generate pEGFP-CaMKIβ and pEGFP-CaMKIδ. All constructs were verified by sequencing.

Gene targeting, neuronal culture, and pharmacology. All animal experiments in this study were performed in accordance with regulations and guidelines for the care and use of the experimental animals of the University of Tokyo, and approved by the institutional review committee of University of Tokyo Graduate School of Medicine.

CaMKKα-knock-out (KO) mice were described previously (Blaeser et al., 2006). CaMKKβ-KO mice were produced similarly by deleting exon 2 (where the ATG starts) through exon 6 of the CaMKKβ gene. A detailed characterization of CaMKKβ-KO mice will be described elsewhere (F. Blaeser and T. A. Chatila, unpublished observations). CaMKKα- and CaMKKβ-KO mice were crossed to produce CaMKKα/β-double knock-out (DKO) mice. The targeting strategy of CaMKIγ/CL3-KO mice was as described previously (Takemoto-Kimura et al., 2007).

Dissociated cortical neurons were prepared and cultured from embryonic day 19 (E19) Sprague Dawley rats or E17 C57BL/6 mice (wild-type as well as mutant mice), essentially as described previously (Takemoto-Kimura et al., 2007). In brief, dissected cortices were incubated for 10 min with 10 mg/ml trypsin type XI (Sigma-Aldrich) plus 0.5 mg/ml DNase I type IV (Sigma-Aldrich) at room temperature and mechanically dissociated in Hanks solution, pH 7.4 (Sigma-Aldrich), with 0.5 mg/ml DNase I type IV and 12 mM $MgSO_4$. Cortical neurons were transfected immediately after dissociation by electroporation using a Nucleofector (Amaxa Biosystems), plated onto poly-L-lysine-coated 12 mm coverslips (BD Biosciences), poly-D-lysine-coated glass-bottom dishes (MatTek) or six-well dish (BD Biosciences), and maintained in minimum essential medium (Invitrogen) containing 5 g/L glucose, 0.2 g/L $NaHCO_3$, 0.1 g/L transferrin (Calbiochem), 2 mM GlutaMAX-I (Invitrogen), 25 μg/ml insulin (Sigma-Aldrich), B-27 supplement (Invitrogen), and 10% fetal bovine serum. Cultures were maintained in 5% CO_2 at 37°C.

For inhibition and stimulation experiments, 2-[*N*-(2-hydroxyethyl)-*N*-(4-methoxybenzenesulfonyl)] amino-*N*-(4-chlorocinnamyl)-*N*-methylbenzylamine (KN-93) (Calbiochem), 1,8-naphthoylene benzimidazole-3-carboxylic acid (STO-609) (Tocris Bioscience), mevastatin (Wako), muscimol (Tocris Bioscience), or BDNF [generously provided by Dainippon Sumitomo Pharma Co., Ltd. (Osaka, Japan) by courtesy of Dr. Chikao Nakayama] were added to the medium of cultured neurons expressing mRFP1 at 6 h after plating at the final concentrations of 10 μM (KN-93), 2.6 μM (STO-609), 10 μM (mevastatin), 1 μM (muscimol), and 50 ng/ml (BDNF), respectively. Bath application was performed by dissolving the reagents in one-half volume of the conditioned culture medium and by mixing this gently with the remaining one-half of the original medium in the dish. No medium change was done onward until fixation.

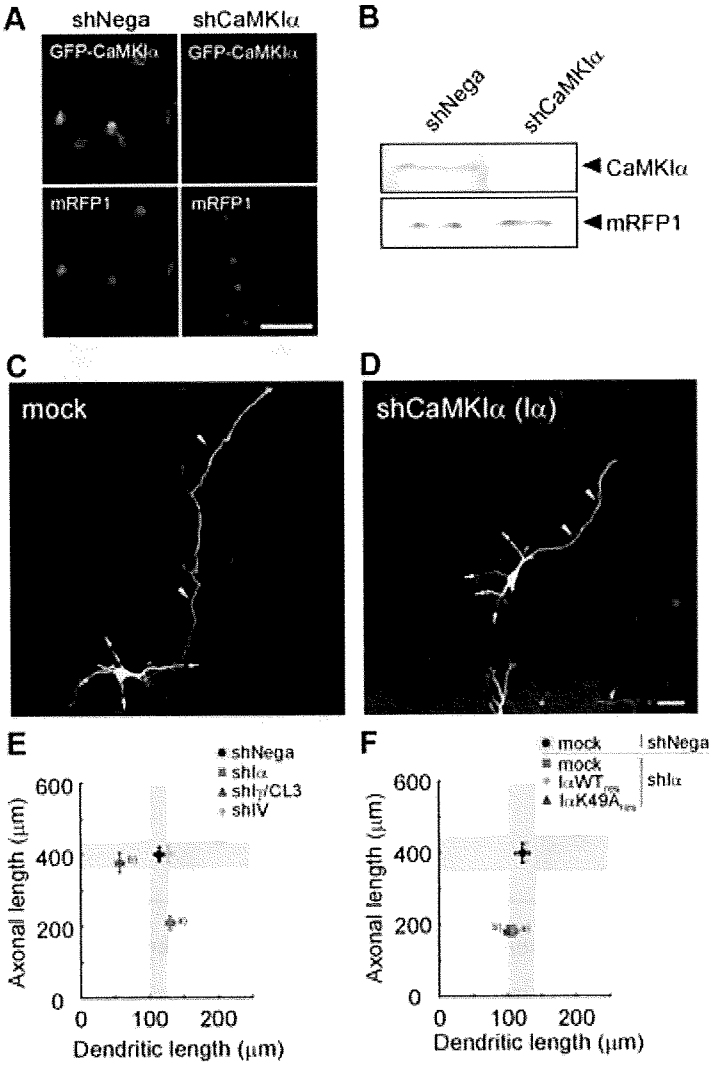

Figure 2. Knockdown of CaMKIα specifically impairs axonal but not dendritic growth. ***A***, Efficient downregulation of exogenous GFP-CaMKIα was achieved by a CaMKIα-targeted shRNA vector (shCaMKIα), but not by a control vector (shNega), in rat cortical neurons. The mRFP1 expression, which was driven by a dual promoter in a pSUPER + mRFP1 vector, remained unchanged. Scale bar, 50 μm. ***B***, Knockdown of endogenous CaMKIα was evaluated by Western blot analysis using an anti-CaMKIα antibody. Rat cortical neurons were transfected with pSUPER-shNega or pSUPER-shCaMKIα by electroporation, and the cells were lysed at 2 DIV. shCaMKIα suppressed endogenous CaMKIα, whereas the control mRFP1 expression level remained unchanged. ***C***, ***D***, shCaMKIα-expressing rat cortical neurons (shCaMKIα) (***D***) showed impaired axonal growth (arrowheads), whereas the dendritic morphology was spared (arrows) compared with neurons from shNega-expressing rat cortical neurons (shNega) (***C***). Scale bar, 25 μm. ***E***, An orthogonal plot of averaged data; $n = 15$ for all groups. [a]Axon, $p < 0.001$. [b]Dendrite, $p < 0.001$ (one-way ANOVA with Tukey's test comparison with shNega). Scale bar, 25 μm. ***F***, Introduction of shCaMKIα-resistant wild-type GFP-CaMKIα (WT_{res}) successfully rescued the axonal defect elicited by shCaMKIα. In contrast, an shCaMKIα-resistant kinase-inactive GFP-CaMKIα (a $K49A_{res}$ point mutant) was unable to rescue the shCaMKIα phenotype. $n = 15$ for all groups. [a,b]Axon, $p < 0.001$ (one-way ANOVA with Tukey's test comparison with shNega + mock).

Immunocytochemistry, morphometric analyses, and visualization of raft-targeted proteins. For morphometric analysis, cortical neurons were transfected immediately after dissociation by electroporation using Nucleofector and plated onto 12 mm poly-L-lysine-coated coverslips at the density of 5×10^5 cells (rats) or 7.5×10^5 cells (mice) per coverslip in 24-well plates. Dissociated cultures of rat and mouse cortical neurons and all measurements (axonal and dendritic length, axonal tip numbers) were performed at 2 d *in vitro* (DIV) essentially as described previously

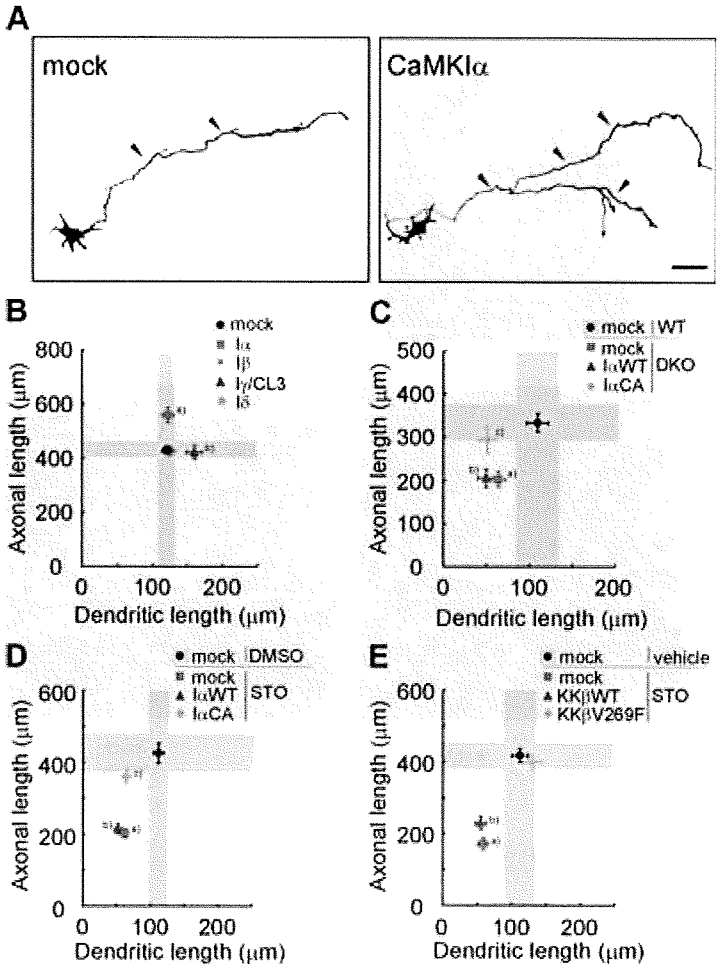

Figure 3. A specific role for a CaMKK–CaMKIα cascade in promoting axonal growth in cortical neurons. ***A***, Representative images of rat cortical neurons transfected with GFP-CaMKIα. Scale bar, 50 μm. ***B***, Overexpression of CaMKIα and CaMKIγ facilitated axonal and dendritic growth, respectively. $n = 15$ for all groups. [a]Axon, $p < 0.001$; [b]dendrite, $p < 0.05$ (one-way ANOVA with Tukey's test comparison with mock). ***C***, The axonal growth defect in DKO mice was selectively rescued by coexpression of a constitutively active CaMKIα (CaMKIαCA), but not by a wild-type CaMKIα (CaMKIαWT); the dendritic growth defect was left unaltered; $n = 15$ for all groups. [a]Axon, $p < 0.01$; dendrite, $p < 0.05$; [b]axon, $p < 0.01$; dendrite, $p < 0.001$; [c]dendrite, $p < 0.01$ (one-way ANOVA with Tukey's test comparison with WT plus mock). ***D***, Only the axonal growth defects caused by STO-609 treatment were rescued by expression of a constitutively active CaMKIα (CaMKIαCA), but not of a wild-type CaMKIα (CaMKIαWT). Dendritic growth defects remained unchanged; $n = 15$ for all groups. [a,b]Axon, $p < 0.001$; dendrite, $p < 0.001$; [c]Dendrite, $p < 0.001$ (one-way ANOVA with Tukey's test comparison with DMSO plus mock). ***E***, Both axonal and dendritic growth defects caused by STO-609 treatment were rescued by introducing an STO-609-resistant CaMKKβ mutant (V269F), but not a CaMKKβ-WT. n = 15 for all groups. [a,b]Axon, $p < 0.001$; dendrite, $p < 0.01$ (one-way ANOVA with Tukey's test comparison with vehicle plus mock).

(Takemoto-Kimura et al., 2007). Images of neuronal morphologies were captured based on immunoreactivities against GFP, mRFP1, or mCherry, using the Olympus BX51 microscopy system with a 20× objective. Dendrites and axons were identified by standard morphological criteria as described previously (Takemoto-Kimura et al., 2007), and only neurons that possessed one clearly classifiable axon and one or more dendrites were analyzed. All quantitative analyses were performed by an observer blinded to the identity of the transfected constructs, genotypes of mice, or treated drugs.

Immunostaining was performed as described previously (Bito et al., 1996; Nonaka et al., 2006; Takemoto-Kimura et al., 2007). A rabbit anti-DsRed antibody (Takara) was used for quantitative morphometric analyses of RNAi, rescue, and forced expression experiments, and a rat anti-GFP antibody (Nacalai Tesque) was used to detect coexpressed constructs. An anti-GM130 antibody (BD Biosciences Transduction Laboratories) was used as a Golgi marker. As secondary antibodies, Alexa 488-, Alexa 594-conjugated anti-mouse, anti-rabbit, and anti-rat IgG antibodies (Invitrogen) were used. Fluorescent images were taken by a confocal laser microscopy system (LSM 510META-V3.2; Carl Zeiss) built on an inverted microscope (Axiovert 200M; Carl Zeiss) with the 40× objective [Plan-Neofluar 40×/numerical aperture (NA) 1.3, oil; Carl Zeiss] or using a CCD camera-based imaging analysis system (an Olympus BX51 equipped with a DP-70 camera). Visualization of raft-targeted proteins was performed as described previously (Takemoto-Kimura et al., 2007).

Western blot analysis. For Western blot analysis, cortical neurons were transfected with pSUPER-shNega or pSUPER-shCaMKIα by electroporation using a Nucleofector and plated at a density of 5×10^6 cells in a six-well dish. At 2 DIV, the cells were lysed in lysis buffer containing 50 mM Tris-HCl, pH 6.8, 2% SDS, and 10% glycerol. A rabbit anti-CaMKIα antibody (Uezu et al., 2002) was used (a kind gift from Drs. Kohji Fukunaga and Jiro Kasahara, Tohoku University, Sendai, Japan). Chemiluminescence detection was performed using horseradish peroxidase-conjugated anti-rabbit IgG and ECL Plus reagent (GE Healthcare).

Calcium imaging. Fluorescent calcium imaging was performed essentially as described previously (Furuyashiki et al., 2002; Takemoto-Kimura et al., 2007). Twenty-four hours after plating, cortical neurons on glass-bottom dishes were loaded with Fluo-4 AM (2.5 μM; Dojindo Laboratories) for 30 min at room temperature. After wash, cells were incubated at 37°C in a stage CO_2 chamber (Tokai Hit Co., Ltd.) equipped on an LSM 510 META (Carl Zeiss). After baseline recording, a medium containing 20× muscimol (final concentration, 1 μM) was gently bath-applied. Fluorescence changes in the cell bodies of individual cells were analyzed using MetaMorph or ImageJ software, and data are expressed as $\Delta F/F_o$.

In utero *electroporation, data acquisition, and quantification of the terminal arborization of callosal axons. In utero* electroporation was performed as described previously (Mizuno et al., 2007). Equal amount of pSUPER-vectors (2 μg/μl) and pCAG-EGFP (2 μg/μl) were mixed together with the dye Fast Green (0.05%; Wako) for injection into the lateral ventricle. The postnatal brains [postnatal day 16 (P16)] were fixed by transcardial perfusion of 4% PFA in 0.1 M phosphate buffer followed by overnight immersive fixation in 4% PFA in PBS and then transferred to 30% sucrose in PBS for 1–2 d at 4°C. Serial coronal brain sections were prepared at 50 μm thickness by a cryostat (HM560; Microm), and every one section out of four was immunostained. Sections were permeabilized in 0.3% Triton X-100 in PBS, and then blocked in 5% normal goat serum, 1% BSA, and 0.3% Triton X-100 in PBS followed by fluorescent immunostaining of EGFP. Sections were counterstained with DAPI (4′,6′-diamidino-2-phenylindole) (Invitrogen). Quantitative analyses were performed and compared using the utmost posterior section of the stained sets that included the corpus callosum.

Confocal images were taken (LSM 510META-V3.2; Carl Zeiss) with a 10× objective (Plan-Neofluar 10×/NA 0.3; air; Carl Zeiss) with 10 μm optical sectioning. *Z* projection images taken at 512 × 512 pixels were acquired by average projection mode and background was subtracted, and the intensity was normalized by maximal intensity in the white mat-

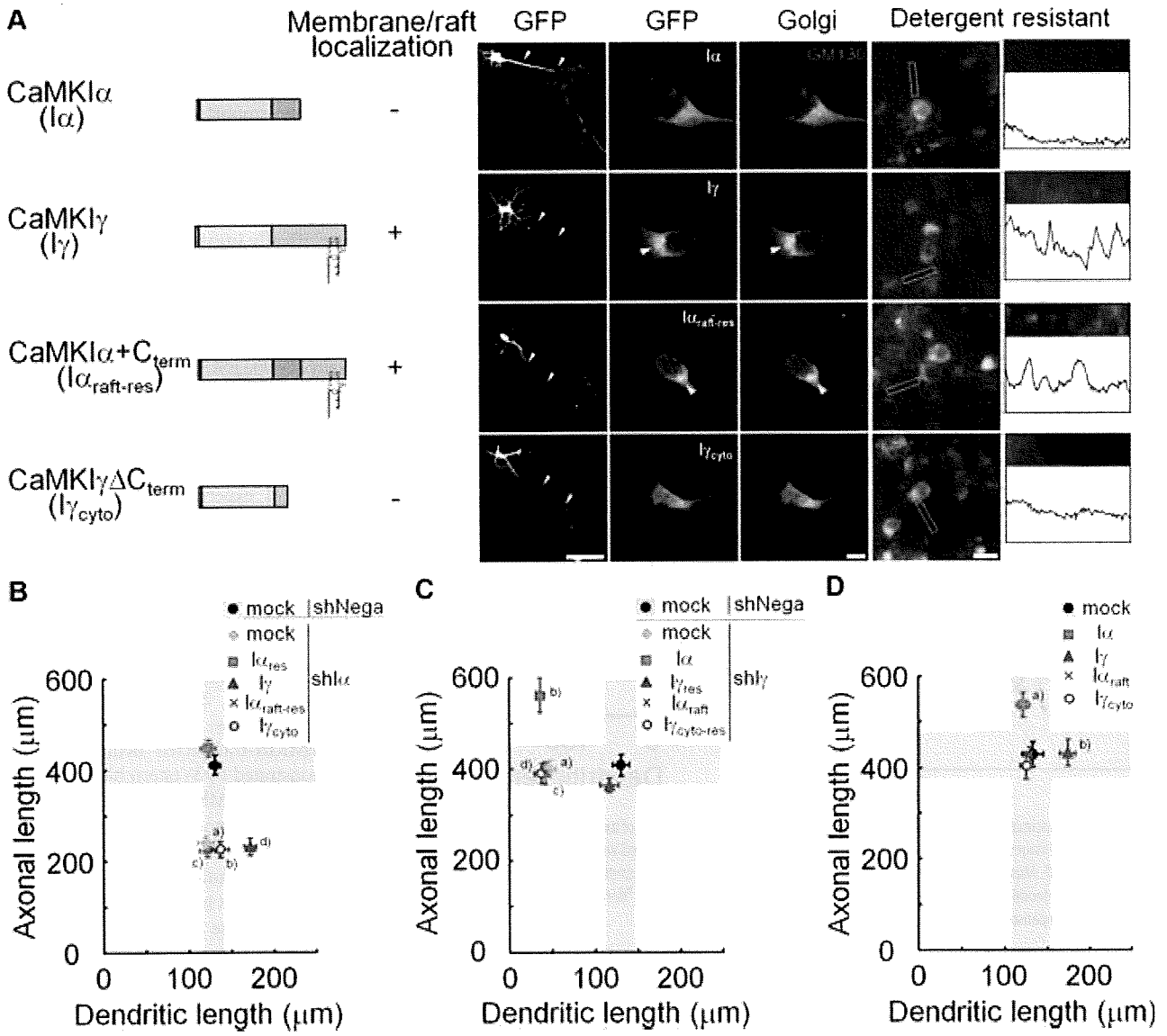

Figure 4. Functional segregation of CaMKK–CaMKIα and CaMKK–CaMKIγ cascades. ***A***, The domain structures and subcellular localizations of CaMKIα (Iα), CaMKIγ/CL3 (Iγ), and their chimeras. GFP-CaMKIα (Iα), CaMKIγ/CL3 (Iγ), and their chimeras distribution detected by anti-GFP immunostaining showed colocalization with a Golgi marker, GM130. GFP-Iγ and $I\alpha_{raft\text{-}res}$ signals were also enriched within Golgi (arrowheads). Single representative confocal sections are shown for Golgi localization. GFP-Iγ and -$I\alpha_{raft\text{-}res}$ fluorescence was retained after detergent treatment in a punctate manner in 2 DIV cortical neurons along the dendrites, demonstrating a sizable portion of detergent-resistant GFP-Iγ and $I\alpha_{raft\text{-}res}$ in the dendritic rafts. Line scans of pixel fluorescence, performed within a chosen field of a 15 μm dendritic segment. Scale bars: right, 50 μm; middle, 5 μm; left, 100 μm. ***B***, Neither Iγ, $I\alpha_{raft\text{-}res}$, nor $I\gamma_{cyto}$ were able to rescue the axonal phenotype caused by knockdown of CaMKIα; $n = 15$ for all groups. ^{a,b,c}Axon, $p < 0.001$; ^{d}axon, $p < 0.001$, dendrite, $p < 0.01$ (one-way ANOVA with Tukey's test comparison with shNega plus mock). ***C***, Neither Iα, $I\alpha_{raft}$, nor $I\gamma_{cyto\text{-}res}$ were able to rescue the dendritic phenotype caused by knockdown of CaMKIγ/CL3; $n = 15$ for all groups. ^{a,c,d}Dendrite, $p < 0.001$; ^{b}axon, $p < 0.001$, dendrite, $p < 0.001$ (one-way ANOVA with Tukey's test comparison with shNega plus mock). ***D***, Overexpression of CaMKIα, specifically increased axon length in cortical neurons; $n = 15$ for all groups; $n = 15$ for all groups. ^{a}Axon, $p < 0.05$; ^{b}dendrite, $p < 0.001$ (one-way ANOVA with Tukey's test comparison with mock).

ter. For one-dimensional fluorescence intensity profile analysis in Figure 7*C*, a rectangular zone (nominal width set at 100 pixels) was drawn along the vertical axis from the pial surface to the white matter, and the average pixel intensity projected onto the vertical axis was calculated. To quantify the impairment of the cortical wiring in Figure 7*D*, average intensity in a rectangle region (100 pixels in width) in the cortex was divided by that in the white matter. Three to five pups were used for quantification. All calculations were performed using MetaMorph software (version 7; Molecular Devices).

Statistical analyses. Statistical analyses were run separately for axonal and dendritic datasets throughout our study, while using scattered diagrams of paired data of axonal and dendritic lengths ("orthogonal plots"). Statistical analyses were performed using Prism 4.0 (GraphPad Software). Student's *t* test was used for comparisons of two groups. One- or two-way ANOVA with *post hoc* Tukey–Kramer or Bonferroni's test was used for factorial analysis among more than three groups. Kolmogorov–Smirnov test was applied to Figure 1, *C* and *D*. All data are shown as mean ± SEM, unless otherwise mentioned, and shaded regions in orthogonal plots graphically depict the zone of mean ± 2SEM on both axes to facilitate the evaluation of the phenotypes.

Results

CaMKK pathway regulates axonal and dendritic growth during early stages of cortical development

We previously reported that a dendritic raft-anchored CaMKIγ/CL3 (Takemoto-Kimura et al., 2003) plays an essential role in

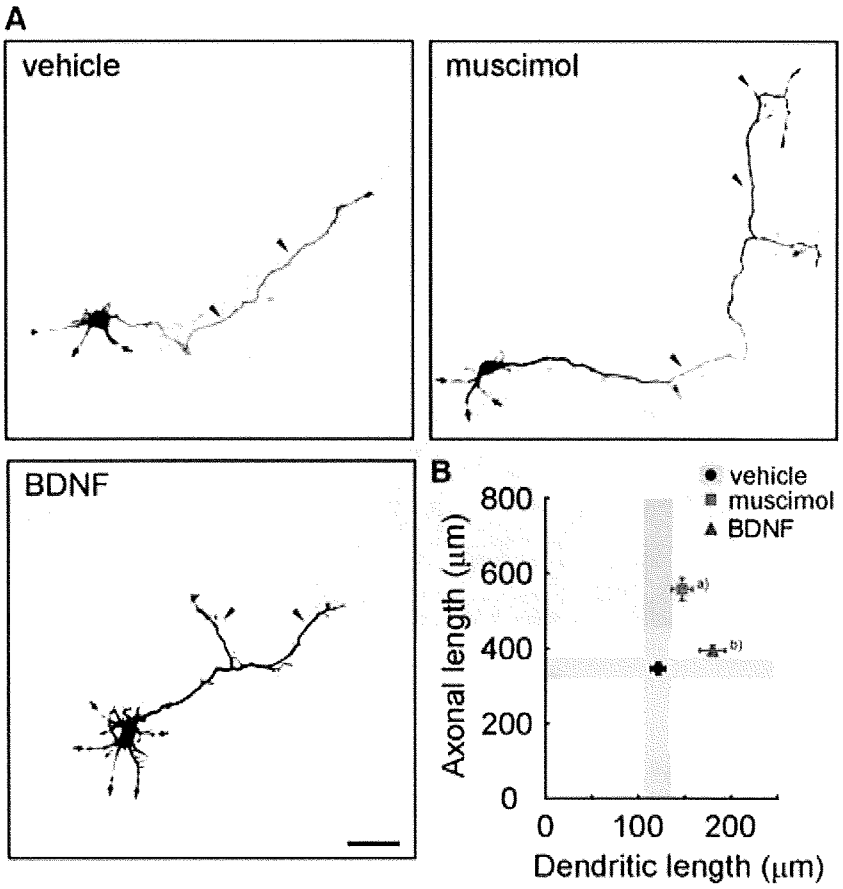

Figure 5. Muscimol, a $GABA_A$ receptor agonist, specifically stimulates elongation of axons in cultured cortical neurons. ***A***, ***B***, Representative images (***A***) and ensemble data (***B***) of immature cortical neurons treated with either muscimol (a $GABA_A$ receptor agonist) or BDNF. Muscimol significantly promoted axonal growth (arrowheads). In contrast, BDNF had no effect on axons but mainly affected dendrites. Scale bar, 50 μm. $n = 15$ for all groups. [a]Axon, $p < 0.001$; [b]dendrite, $p < 0.01$ (one-way ANOVA with Tukey's test comparison with vehicle).

dendritic growth downstream of BDNF during the morphological maturation of cortical neurons (Takemoto-Kimura et al., 2007). As four distinct CaMKI isoforms (α, β, γ/CL3, and δ) and CaMKIV are activated by upstream CaMKKs α and β, we sought to test how potently neuritogenesis was disturbed in cultured cortical neurons generated from CaMKKα/β-DKO mice. To specifically identify the genotype contribution to either axonal or dendritic growth, we orthogonally plotted the dendritic length (i.e., total length of all dendritic processes) and axonal length (i.e., total length of all axonal processes including branches) for each GFP-expressing cortical neuron blindly chosen from multiple fields of view (Fig. 1*A*,*B*; supplemental Fig. 1, available at www.jneurosci.org as supplemental material). Although cortical neurons from CaMKIγ/CL3 knock-out mice revealed a strikingly dendrite-specific deficit (Fig. 1*A–D*), we found that both axons and dendrites were significantly shortened in cortical neurons from DKO mice, compared with neurons from WT mice (Fig. 1*A–F*). Exposure to KN-93, which blocks all CaMK species (CaMKII, CaMKI, CaMKIV, and CaMKK), also reduced both total axonal and dendritic lengths (Fig. 1*G*,*H*). Specific blockade of the CaMKKs, using STO-609, a selective inhibitor for CaMKKs (Tokumitsu et al., 2002), resulted in a quantitatively similar impairment (Fig. 1*G*,*H*). Together, these genetic and pharmacological experiments clearly demonstrated that CaMKK-mediated CaMK cascades played critical roles both in axonogenesis and dendritogenesis of immature cortical neurons, consistent with a previous work on other cell types (Wayman et al., 2004). Furthermore, our data pointed to the presence of a selective CaMKK–CaMK cascade that strongly supported cortical axonal growth in a manner that was distinct from the dendritic contribution of CaMKIγ.

Suppression of CaMKIα expression specifically impairs axonal but not dendritic growth

To identify which of CaMKI or CaMKIV isoform(s) was involved in regulation of the axonal growth, we designed several short hairpin-type pSUPER vectors that were targeted to specific isoforms of the CaMKI/IV subfamily members. In this RNAi experiment, we also coexpressed a PGK promoter-driven mRFP1 as a morphological tracer. In a control experiment, polarized cortical neurons grown for 48 h typically grew 5~6 dendrites and a single axon. Knockdown using an shCaMKIα vector was prominent enough such that even an overexpressed GFP-CaMKIα became barely detectable 48 h after transfection, whereas the control mRFP1 expression level remained unchanged (Fig. 2*A*). Strong suppression of endogenous CaMKIα expression in shCaMKIα-transfected neurons was also demonstrated by Western blot analysis using an anti-CaMKIα antibody (Fig. 2*B*). A lack of cross-knockdown effects across α-, γ-CaMKI isoforms and CaMKIV was verified (supplemental Fig. 2, available at www.jneurosci.org as supplemental material).

Under these conditions, shCaMKIα-treated neurons showed unchanged dendritic growth but had a markedly shorter axon (Fig. 2*C*,*D*). Under the same conditions, in contrast, CaMKIγ/CL3 knockdown specifically blocked dendritic, but not axonal, outgrowth (Fig. 2*E*) (Takemoto-Kimura et al., 2007), whereas CaMKIV knockdown had no effect (Fig. 2*E*). The striking specificity in the axonal phenotype of CaMKIα was replicated even when axonal growth was measured under conditions in which shCaMKIα-transfected neurons were kept in suspension culture for an extended period (48 h) before plating, to ensure a maximized knockdown efficiency (supplemental Fig. 3, available at www.jneurosci.org as supplemental material). The impairment in axonal growth observed in CaMKIα-diminished neurons was rescued by expression of an shCaMKIα-resistant WT-CaMKIα (WT_{res}), but not by that of an shCaMKIα-resistant kinase-inactive CaMKIα ($K49A_{res}$), demonstrating the requirement of the kinase activity of CaMKIα (Fig. 2*F*). Together, our results strongly implicated the CaMKK–CaMKIα cascade as a critical player in the control of cortical axonal growth.

Two separate CaMKK–CaMKI cascades control cortical axonal and dendritic growth

In keeping with this robust selectivity in the knockdown experiments, forced expression of either one of the four CaMKI isoforms revealed that total axonal length was stimulated only by an

increase in CaMKIα, whereas dendrite growth was promoted only by CaMKIγ/CL3 expression (Fig. 3*A*,*B*). No change in primary axon number was detected in CaMKIα-overexpressing neurons, suggesting that CaMKIα did not act on axon specification per se (data not shown). Most critically, expression of a constitutively active CaMKIα (CaMKIαCA), was sufficient to rescue the axonal deficit, but without altering dendritic atrophy, in cortical neurons from DKO mice (Fig. 3*C*) or in WT neurons treated with STO-609 (Fig. 3*D*). However, forced expression of CaMKIαWT, which enzymatically remains inactive in the absence of CaMKK activity, had no effect in either of these backgrounds (Fig. 3*C*,*D*). In a parallel experiment, both axonal and dendritic defects in WT neurons treated with STO-609 were rescued by transfection of a STO-609-resistant CaMKKβ V269F mutant (Tokumitsu et al., 2003) (Fig. 3*E*).

Together, these data strongly implicated the CaMKK–CaMKIα and CaMKK–CaMKIγ cascades as parallel pathways acting independently in the promotion of axonal and dendrite growth, respectively, in cultured cortical neurons.

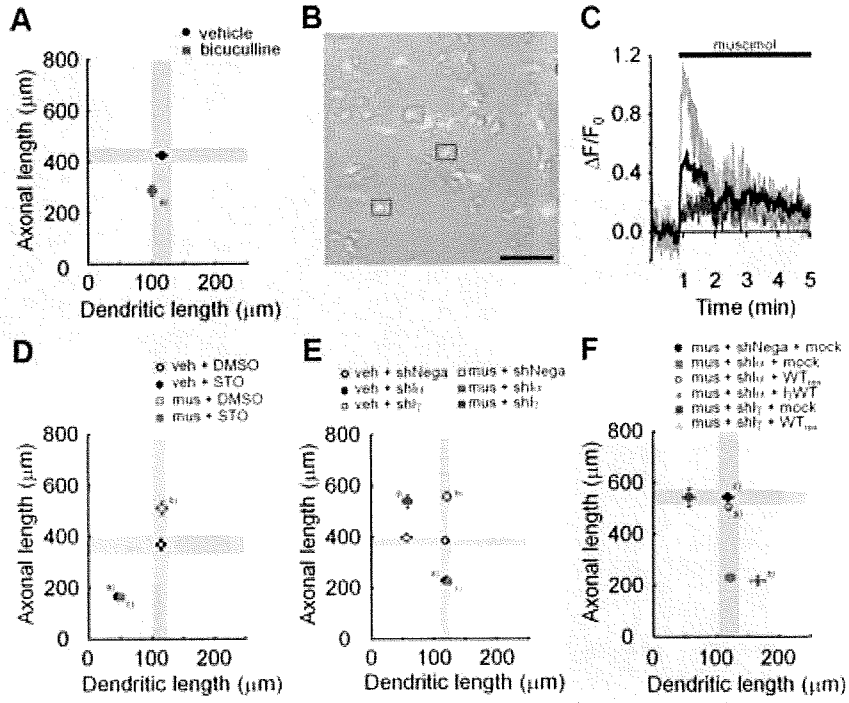

Figure 6. Activation of $GABA_A$ receptors promotes axonal growth via the CaMKK–CaMKIα pathway in immature cortical neurons. ***A***, Bicuculline, a $GABA_A$ receptor antagonist, blocked axonal growth; $n = 15$ for all groups. [a]Axon, $p < 0.001$ (Student's *t* test comparison with vehicle). ***B***, Embryonic cortical neurons (1 DIV) were loaded with a calcium indicator, Fluo-4 AM, and calcium responses were measured by time-lapse imaging. A green fluorescence image was overlaid on a differential interference contrast image. The colored boxes indicate the location of cells shown in ***C***. Scale bar, 50 μm. ***C***, Representative calcium responses in individual cells after muscimol administration. Three different types of calcium responses were revealed (green, blue, and red). An averaged response from 10 cells in a microscopic field is revealed in black. ***D***, Both basal and muscimol-stimulated axonal growths were suppressed with STO-609, a specific blocker of CaMKKα/β; $n = 15$ for all groups. Axon: two-way ANOVA, muscimol effect, $F_{(1,56)} = 14.38, p = 0.0004$; drug effect, $F_{(1,56)} = 225.63, p < 0.0001$; muscimol × drug, $F_{(1,56)} = 15.79, p = 0.0002$. Dendrite: two-way ANOVA, muscimol effect, $F_{(1,56)} = 0.39$, $p = 0.5336$; drug effect, $F_{(1,56)} = 105.76$, $p < 0.0001$; muscimol × drug, $F_{(1,56)} = 0.13, p = 0.7199$. [a,b]Axon, $p < 0.001$ (comparison with vehicle plus DMSO); [c]axon, $p < 0.001$ (comparison with muscimol plus DMSO); n.s. (comparison with vehicle plus STO). ***E***, CaMKIα knockdown quantitatively inhibited axonal growth induced by muscimol treatment, to an extent similar to that obtained with STO-609; $n = 15$ for all groups. Axon: two-way ANOVA, muscimol effect, $F_{(1,84)} = 66.44, p < 0.0001$; RNAi effect, $F_{(2,84)} = 168.04, p < 0.0001$; muscimol × RNAi, $F_{(2,84)} = 19.96, p < 0.0001$. Dendrite: two-way ANOVA, muscimol effect, $F_{(1,84)} = 0.23, p = 0.6305$; RNAi effect, $F_{(2,84)} = 61.58$, $p < 0.0001$; muscimol × RNAi, $F_{(2,84)} = 0.01$, $p = 0.9888$. [a,b]Axon, $p < 0.001$ (comparison with vehicle plus shNega); [c]axon, $p < 0.001$ (comparison with muscimol plus shNega); n.s. (comparison with vehicle plus shIα); [d]axon, $p < 0.001$ (comparison with vehicle plus shIγ); n.s. (comparison with muscimol plus shNega). ***F***, Introduction of shCaMKIα-resistant wild-type GFP-CaMKIα (WT_{res}) specifically rescued the suppression of muscimol-induced axonal growth triggered by knockdown of CaMKIα; $n = 15$ for all groups. [a]Axon, $p < 0.001$; dendrite, n.s.; [b]axon, n.s.; dendrite, $p < 0.001$ (one-way ANOVA with Tukey's test comparison with muscimol plus shIα plus mock); [c]axon, n.s.; dendrite, $p < 0.001$ (*t* test comparison with muscimol plus shIγ plus mock).

Both localization and kinase specificity of CaMKIα play important roles in CaMKIα-dependent axonal growth

Our data, so far, suggested that the axonogenic action of CaMKIα manifested in a manner that was completely orthogonal and independent to the dendritogenic effect mediated by CaMKIγ/CL3, despite a high degree of structural identity (71% amino acid identity in the catalytic domain sequences). What then discriminated the distinct function of these two kinases?

To identify the molecular determinants involved in axonogenic and dendritogenic selectivity of the CaMKK–CaMKI cascades, we generated CaMKIα/γ chimeras such that each kinase domain was paired with either cytosolic or Golgi/raft localization signals in the C terminus (Fig. 4*A*) (Takemoto-Kimura et al., 2007). We then tested their potencies to rescue the defect caused by knockdown of endogenous CaMKIα. As expected, forced expression of an shCaMKIα-resistant WT-CaMKIα ($Iα_{res}$) rescued the axonal impairment in CaMKIα knockdown neurons (Fig. 4*B*). The WT-CaMKIγ/CL3 (Iγ), however, promoted dendritic growth without showing any effect on axonal deficit. CaMKIα is believed to be freely diffusible. However, the C-terminal region of CaMKIγ/CL3 is lipidified by prenylation and palmitoylation, targeting it preferentially into lipid rafts, which are highly abundant in dendrites and in Golgi (Takemoto-Kimura et al., 2007) (Fig. 4*A*; supplemental Fig. 4, available at www.jneurosci.org as supplemental material). A dendritic raft-targeted mutant of CaMKIα, GFP-CaMKIα+C_{term} ($Iα_{raft\text{-}res}$), was unable to rescue the axonal impairment in CaMKIα knockdown neurons (Fig. 4*B*). A cytoplasmic, raft-excluded mutant of CaMKIγ/CL3, namely CaMKIγ/ CL3ΔC_{term} ($Iγ_{cyto}$), had no ability, either (Fig. 4*B*), contrary to our expectations. Thus, surprisingly, CaMKI-mediated selectivity of neurite growth might not be simply determined by the localization of a CaMKIα or CaMKIγ in or out of the membrane rafts.

To further confirm this, the chimeras were expressed in the background of CaMKIγ/CL3-knockdown neurons. Expression of an RNAi-resistant WT-CaMKIγ/CL3 ($Iγ_{res}$) rescued the dendritic impairment, whereas WT-CaMKIα (Iα) promoted axonal growth without an effect on dendrite impairment (Fig. 4*C*). Again, however, neither a freely diffusible CaMKIγ/CL3ΔC_{term} ($Iγ_{cyto\text{-}res}$), nor a raft-targeted CaMKIα, CaMKIα+C_{term} ($Iα_{raft}$), had any effect (Fig. 4*C*). Furthermore, forced expression of CaMKIα, CaMKIγ, and CaMKIα/γ chimeras in a naive background revealed that total axonal length was stimulated only by

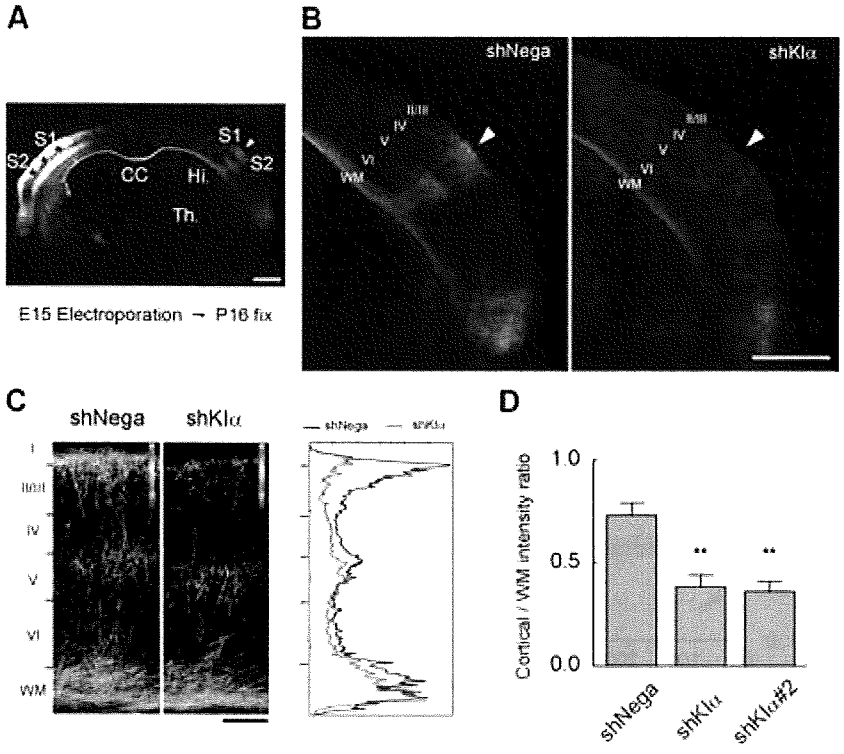

Figure 7. Knockdown of CaMKIα impairs terminal extension of callosal axons *in vivo*. ***A***, A control coronal section was obtained near the posterior end of the corpus callosum, from a P16 pup electroporated *in utero* with pSUPER-shNega and pCAG-EGFP on E15.5. The somatodendritic regions of layer II/III neurons were strongly labeled (asterisks) in the somatosensory cortex, from which callosal axons projected toward the contralateral cortical areas at the S1/S2 border region (arrowhead). Scale bar, 1 mm. CC, Corpus callosum; Hi, hippocampus; Th, thalamus. ***B***, Terminal extension of callosal axons into the contralateral cortical layers was severely disrupted in CaMKIα-knockdown neurons (shKIα), although axons were able to reach the white matter (WM) beneath S1/S2 area (arrowhead). Scale bar, 1 mm. ***C***, Axonal extension and terminal branch arborization were strongly impaired in layers II/III in CaMKIα-knockdown neurons, as illustrated by the magnified images of GFP marker showing the total axonal volumes present in the cortical layers (in pseudocolor), or by a one-dimensional fluorescence intensity profile analysis. Scale bar, 200 μm. ***D***, Quantification of the cortical wiring defect caused by an aberrant terminal axon extension in the cortex. Two independent RNAi constructs (shKIα and shKIα #2) gave similar results. $^{**}p < 0.01$ (one-way ANOVA with Tukey's test comparison with shNega).

an increase in CaMKIα (Fig. 4*D*). Together, these data provide strong functional evidence in support of the notion that CaMKK–CaMKIα and CaMKK–CaMKIγ are not duplicative mechanisms with simply altered targeting of downstream kinases, but are genuinely segregated cascades that are divergent at the level of kinase substrate specificity.

GABA is one of the physiological ligand acting upstream of CaMKIα to promote axonal growth during early stages of cortical development

The biological significance of this specificity could be demonstrated if the physiological signal triggering the axonogenic effect of CaMKIα was identified. To this end, we searched for a potential extracellular ligand that induced intracellular calcium elevation and potently stimulated axonal growth. We found that muscimol, a $GABA_A$ receptor agonist with a known excitatory action during perinatal development (Owens et al., 1996; Represa and Ben-Ari, 2005), specifically promoted elongation of axons, but not of dendrites, in cultured cortical neurons (Fig. 5*A*,*B*). Under the same conditions, we confirmed that BDNF had a complementary growth effect mostly selective for dendrites (Takemoto-Kimura et al., 2007).

To test the extent of requirement for GABA, we added bicuculline, a $GABA_A$ receptor antagonist, in the medium and found that axonal growth was rather selectively impaired (Fig. 6*A*). Furthermore, we confirmed that muscimol application triggered a strong Ca^{2+} influx in our cortical neurons (Fig. 6*B*,*C*). In keeping with this, forced expression of KCC2, a neuronal K^+/Cl^- cotransporter that lowers intracellular Cl^- concentration, and that is upregulated during development to convert the GABA action from excitation to inhibition (Rivera et al., 1999), impaired both constitutive and muscimol-stimulated axonal growth (supplemental Fig. 5, available at www.jneurosci.org as supplemental material). Pharmacological blockade of all CaM kinases using KN-93 (supplemental Fig. 6, available at www.jneurosci.org as supplemental material), or of CaMKK using STO-609 (Fig. 6*D*), completely blocked the axonogenic muscimol effect. CaMKIα RNAi (shIα), but not CaMKIγ/CL3 RNAi (shIγ), selectively impaired muscimol-stimulated axonal growth (Fig. 6*E*), and this effect was rescued by coexpressing an shCaMKIα-resistant CaMKIα WT ($I\alpha WT_{res}$), but not CaMKIγ/CL3 WT (IγWT) (Fig. 6*F*). Thus, a CaMKK–CaMKIα cascade may critically mediate $GABA_A$-stimulated axon outgrowth during the early development of a cortical neuron.

Contribution of CaMKIα in fine-tuning axonal pathfinding *in vivo*

We finally tested the *in vivo* relevance of these findings by investigating the function of CaMKIα during activity-dependent cortical wiring *in vivo*. The callosal axons that originate from layer II/III pyramidal neurons of the somatosensory cortex are known to elongate and target themselves to the border between the S1 and S2 areas of the contralateral cortex, where they suddenly turn and grow into the cortical layers and develop their terminal branches mainly at layers II–III and V. Previous reports demonstrated that reduction of neuronal excitability by overexpression of an inwardly rectifying potassium channel, Kir2.1, impaired such layer-specific development of the terminal branches in the visual cortex (Mizuno et al., 2007) and in the somatosensory cortex (Wang et al., 2007). Furthermore, premature elimination of excitatory GABA drive by forced expression of KCC2 or knockdown of NKCC1 in newly born cortical neurons dramatically perturbed the morphological maturation of the dendrites (Cancedda et al., 2007; Wang and Kriegstein, 2008) or of the terminal callosal axon branches (H. Mizuno, T. Hirano, and Y. Tagawa, unpublished data).

If the morphogenetic effect of excitatory GABA required Ca^{2+} signaling, could the CaMKK–CaMKIα pathway perhaps mediate activity-dependent control of callosal axonal extension? To test this, CaMKIα was knocked down in the somatosensory layer II/III neurons by *in utero* electroporation at E15.5, and an effect on axonal growth was examined. At P16, control neurons terminated their axons into a restricted region (border of S1/S2 area) in the contralateral cortex and extensively developed their terminal

branches into layers II/III and V (Fig. 7*A*). CaMKIα-knockdown neurons extended interhemispheric axonal projections in the white matter, suggesting the CaMKIα may not be absolutely required for midline crossing and progression of axon fibers (Fig. 7*B*). However, their terminal axonal extension into the cortical layers was severely diminished, especially in layers II/III (Fig. 7*C*,*D*). These results indicate a developmentally critical role of CaMKIα in activity-dependent regulation of cortical connectivity *in vivo*.

Discussion

Differential control of cortical axonogenesis and dendritogenesis by activation of CaMKIα and CaMKIγ/CL3

In a previous work (Takemoto-Kimura et al., 2007), we showed that a lipid-modified CaM kinase CaMKIγ/CL3 (a membrane-anchored CaMKI isoform) was directed to the dendrites on raft insertion and could potently promote early dendritic development, with little effect on axon outgrowth, in cultured cortical neurons. In striking contrast to CaMKIγ/CL3, we here demonstrate that a cytosolic sister kinase, CaMKIα, has a complementary role: it has little role in dendritogenesis, but is necessary and sufficient to promote axonogenesis in the same preparation. Additionally, our present work established that CaMKIα regulates axonal extension *in vivo*. Additional rigorous quantitative studies are awaited to establish the potential role of other CaMKK–CaMK signaling pathways in cortical neuritogenesis in general.

How can such specificity of axonal/dendritic growth be regulated by two separate yet structurally resembling kinases lying downstream of the same CaMKKs? The chimeric kinase experiments (Fig. 4) strongly suggested that the diverging kinase substrate specificities and the dissimilarity in subcellular localization (cytosol vs dendritic rafts) might provide a basis for the strikingly differential effect of CaMKIα and CaMKIγ/CL3 during axonal and dendritic development. In support of this functional segregation between the two distinct CaMKK–CaMKI cascades, we identified an extracellular ligand, GABA, which specifically stimulated axonal growth via CaMKIα (this study), whereas BDNF selectively promoted dendritic growth via CaMKIγ (Takemoto-Kimura et al., 2007), during an early developmental stage of cortical neurons.

In principle, BDNF could rather selectively act on dendrites in part because of the strong affinity of the active TrkB receptor to lipid rafts (Suzuki et al., 2004), which are enriched on dendrites. At this point, however, how GABA stimuli could possibly generate an axon-specific effect remains rather unclear, although preliminary Ca^{2+} imaging experiments indicated that $GABA_A$ stimulation might trigger growth cone-localized Ca^{2+} transients (S. Kamijo, H. Fujii, S. Takemoto-Kimura, and H. Bito, unpublished data). It is noteworthy that many potential *in vitro* substrates of CaMKIα have previously been associated with axonal or presynaptic functions. These include synapsin I (Nairn and Greengard, 1987), Numb and Numbl (Tokumitsu et al., 2005), microtubule affinity regulating kinase 2 (MARK2/Par-1b) (Uboha et al., 2007), and β-Pak-interacting exchange factor (βPIX) (Saneyoshi et al., 2008). Although some of these known substrates of CaMKI may potentially underlie a part of early axonal growth, additional work is clearly needed to fully elucidate how an axonogenic substrate may be activated via phosphorylation by CaMKIα.

A pivotal role for a GABA-driven CaMKK–CaMKIα cascade in controlling axonal morphogenesis during early development

In this work, we identified a crucial role for GABA in controlling cortical axon outgrowth during early development via a CaMKK–CaMKIα cascade. In immature cortical neurons, what is the mechanism by which GABA can stimulate axonal development in a CaMKI-dependent manner? Recent studies showed that $GABA_A$ receptors activation has potent excitatory effects in immature, but not in mature, neurons (Ben-Ari et al., 2007). The excitatory action of GABA was demonstrated to be caused by a high basal Cl^- concentration in immature neurons, because of a high amount of the Na^+–K^+–$2Cl^-$ cotransporter (NKCC1) which favors Cl^- influx, whereas the K^+–Cl^- cotransporter (KCC2) primarily responsible for Cl^- efflux is still low in expression (Payne et al., 2003). Because of elevated intracellular Cl^- concentration in immature neurons, $GABA_A$ receptors activation thus induces depolarization (Ben-Ari et al., 2007), thereby likely triggering the opening of voltage-gated Ca^{2+} channels, which then generates enough Ca^{2+} influx leading to CaMKK–CaMKIα activation.

During early development, it is now known that GABA controls a variety of biological processes. Our work has only addressed the significance of the CaMKK–CaMKIα cascade in GABA-mediated cortical axonogenesis during the perinatal period. Whether other GABA-regulated processes may also be mediated by CaMKIα clearly remains to be investigated. For instance, the process of cortical migration has also been reported to be regulated by GABA through signal transduction pathways involving Ca^{2+}, both *in vitro* (Behar et al., 1996, 1998, 2000) and *in vivo* (Heck et al., 2007). Interestingly, treatment with calmidazolium, an inhibitor of calmodulin, reduces the migration rate in cerebellar granule cells (Kumada and Komuro, 2004). Additional studies are needed to determine whether the CaMKK–CaMKIα cascade may play additional roles in such developmental processes as well.

A CaMKK–CaMKIα pathway may regulate fine-sculpting of cortical wiring

We here established the critical importance of an axonogenic GABA–CaMKK–CaMKIα pathway during early development *in vitro*. Moreover, this study indicated that CaMKIα regulated activity-dependent extension of terminal cortical axons *in vivo*. Interestingly, premature elimination of excitatory GABA action by forced expression of KCC2 in newly born cortical neurons dramatically perturbed the morphological maturation of the dendrites (Cancedda et al., 2007) or of the terminal callosal axon branches (H. Mizuno, T. Hirano, and Y. Tagawa, unpublished data). Our present findings thus uncover an unexpected role of the CaMKK–CaMKIα cascade as one key mechanism in GABA-driven activity-dependent regulation of cortical connectivity. More studies are needed to establish whether and how other Ca^{2+}-mobilizing signals (e.g., BDNF) may spatially and temporally interact and perhaps cooperate with such an axonogenic GABA–CaMKK–CaMKIα pathway. Finally, our data lend support to the existence of a perinatal time window of structural refinement, during which spontaneous Ca^{2+} signaling regulated by trophic factors, guidance signals, and ambient neurotransmitters, such as BDNF or GABA, critically fine-tunes cortical connectivity, perhaps even before the receipt of the earliest sensory cues.

References

Behar TN, Li YX, Tran HT, Ma W, Dunlap V, Scott C, Barker JL (1996) GABA stimulates chemotaxis and chemokinesis of embryonic cortical neurons via calcium-dependent mechanisms. J Neurosci 16:1808–1818.

Behar TN, Schaffner AE, Scott CA, O'Connell C, Barker JL (1998) Differential response of cortical plate and ventricular zone cells to GABA as a migration stimulus. J Neurosci 18:6378–6387.

Behar TN, Schaffner AE, Scott CA, Greene CL, Barker JL (2000) GABA receptor antagonists modulate postmitotic cell migration in slice cultures of embryonic rat cortex. Cereb Cortex 10:899–909.

Ben-Ari Y, Gaiarsa JL, Tyzio R, Khazipov R (2007) GABA: a pioneer transmitter that excites immature neurons and generates primitive oscillations. Physiol Rev 87:1215–1284.

Bito H, Takemoto-Kimura S (2003) Ca^{2+}/CREB/CBP-dependent gene regulation: a shared mechanism critical in long-term synaptic plasticity and neuronal survival. Cell Calcium 34:425–430.

Bito H, Deisseroth K, Tsien RW (1996) CREB phosphorylation and dephosphorylation: a Ca^{2+}- and stimulus duration-dependent switch for hippocampal gene expression. Cell 87:1203–1214.

Blaeser F, Sanders MJ, Truong N, Ko S, Wu LJ, Wozniak DF, Fanselow MS, Zhuo M, Chatila TA (2006) Long-term memory deficits in pavlovian fear conditioning in Ca^{2+}/calmodulin kinase kinase alpha-deficient mice. Mol Cell Biol 26:9105–9115.

Cancedda L, Fiumelli H, Chen K, Poo MM (2007) Excitatory GABA action is essential for morphological maturation of cortical neurons *in vivo*. J Neurosci 27:5224–5235.

Dickson BJ (2002) Molecular mechanisms of axon guidance. Science 298:1959–1964.

Furuyashiki T, Arakawa Y, Takemoto-Kimura S, Bito H, Narumiya S (2002) Multiple spatiotemporal modes of actin reorganization by NMDA receptors and voltage-gated Ca^{2+} channels. Proc Natl Acad Sci U S A 99:14458–14463.

Gomez TM, Zheng JQ (2006) The molecular basis for calcium-dependent axon pathfinding. Nat Rev Neurosci 7:115–125.

Heck N, Kilb W, Reiprich P, Kubota H, Furukawa T, Fukuda A, Luhmann HJ (2007) GABA-A receptors regulate neocortical neuronal migration in vitro and in vivo. Cereb Cortex 17:138–148.

Hook SS, Means AR (2001) Ca^{2+}/CaM-dependent kinases: from activation to function. Annu Rev Pharmacol Toxicol 41:471–505.

Hudmon A, Schulman H (2002) Neuronal Ca^{2+}/calmodulin-dependent protein kinase II: the role of structure and autoregulation in cellular function. Annu Rev Biochem 71:473–510.

Ishikawa Y, Tokumitsu H, Inuzuka H, Murata-Hori M, Hosoya H, Kobayashi R (2003) Identification and characterization of novel components of a Ca^{2+}/calmodulin-dependent protein kinase cascade in HeLa cells. FEBS Lett 550:57–63.

Kater SB, Mattson MP, Cohan C, Connor J (1988) Calcium regulation of the neuronal growth cone. Trends Neurosci 11:315–321.

Kumada T, Komuro H (2004) Completion of neuronal migration regulated by loss of Ca^{2+} transients. Proc Natl Acad Sci U S A 101:8479–8484.

Mizuno H, Hirano T, Tagawa Y (2007) Evidence for activity-dependent cortical wiring: formation of interhemispheric connections in neonatal mouse visual cortex requires projection neuron activity. J Neurosci 27:6760–6770.

Nairn AC, Greengard P (1987) Purification and characterization of Ca^{2+}/calmodulin-dependent protein kinase I from bovine brain. J Biol Chem 262:7273–7281.

Nonaka M, Doi T, Fujiyoshi Y, Takemoto-Kimura S, Bito H (2006) Essential contribution of the ligand-binding βB/βC loop of PDZ1 and PDZ2 in the regulation of postsynaptic clustering, scaffolding, and localization of postsynaptic density-95. J Neurosci 26:763–774.

Owens DF, Boyce LH, Davis MB, Kriegstein AR (1996) Excitatory GABA responses in embryonic and neonatal cortical slices demonstrated by gramicidin perforated-patch recordings and calcium imaging. J Neurosci 16:6414–6423.

Payne JA, Rivera C, Voipio J, Kaila K (2003) Cation-chloride co-transporters in neuronal communication, development and trauma. Trends Neurosci 26:199–206.

Represa A, Ben-Ari Y (2005) Trophic actions of GABA on neuronal development. Trends Neurosci 28:278–283.

Rivera C, Voipio J, Payne JA, Ruusuvuori E, Lahtinen H, Lamsa K, Pirvola U, Saarma M, Kaila K (1999) The K^+/Cl^- co-transporter KCC2 renders GABA hyperpolarizing during neuronal maturation. Nature 397:251–255.

Saneyoshi T, Wayman G, Fortin D, Davare M, Hoshi N, Nozaki N, Natsume T, Soderling TR (2008) Activity-dependent synaptogenesis: regulation by a CaM-kinase kinase/CaM-kinase I/betaPIX signaling complex. Neuron 57:94–107.

Schmitt JM, Wayman GA, Nozaki N, Soderling TR (2004) Calcium activation of ERK mediated by calmodulin kinase I. J Biol Chem 279:24064–24072.

Soderling TR (1999) The Ca-calmodulin-dependent protein kinase cascade. Trends Biochem Sci 24:232–236.

Soderling TR, Stull JT (2001) Structure and regulation of calcium/calmodulin-dependent protein kinases. Chem Rev 101:2341–2352.

Suzuki S, Numakawa T, Shimazu K, Koshimizu H, Hara T, Hatanaka H, Mei L, Lu B, Kojima M (2004) BDNF-induced recruitment of TrkB receptor into neuronal lipid rafts: roles in synaptic modulation. J Cell Biol 167:1205–1215.

Takemoto-Kimura S, Terai H, Takamoto M, Ohmae S, Kikumura S, Segi E, Arakawa Y, Furuyashiki T, Narumiya S, Bito H (2003) Molecular cloning and characterization of CLICK-III/CaMKIgamma, a novel membrane-anchored neuronal Ca^{2+}/calmodulin-dependent protein kinase (CaMK). J Biol Chem 278:18597–18605.

Takemoto-Kimura S, Ageta-Ishihara N, Nonaka M, Adachi-Morishima A, Mano T, Okamura M, Fujii H, Fuse T, Hoshino M, Suzuki S, Kojima M, Mishina M, Okuno H, Bito H (2007) Regulation of dendritogenesis via a lipid-raft-associated Ca^{2+}/calmodulin-dependent protein kinase CLICK-III/CaMKIgamma. Neuron 54:755–770.

Tessier-Lavigne M, Goodman CS (1996) The molecular biology of axon guidance. Science 274:1123–1133.

Tokumitsu H, Inuzuka H, Ishikawa Y, Ikeda M, Saji I, Kobayashi R (2002) STO-609, a specific inhibitor of the Ca^{2+}/calmodulin-dependent protein kinase kinase. J Biol Chem 277:15813–15818.

Tokumitsu H, Inuzuka H, Ishikawa Y, Kobayashi R (2003) A single amino acid difference between alpha and beta Ca^{2+}/calmodulin-dependent protein kinase kinase dictates sensitivity to the specific inhibitor, STO-609. J Biol Chem 278:10908–10913.

Tokumitsu H, Hatano N, Inuzuka H, Sueyoshi Y, Yokokura S, Ichimura T, Nozaki N, Kobayashi R (2005) Phosphorylation of Numb family proteins. Possible involvement of Ca^{2+}/calmodulin-dependent protein kinases. J Biol Chem 280:35108–35118.

Uboha NV, Flajolet M, Nairn AC, Picciotto MR (2007) A calcium- and calmodulin-dependent kinase Iα/microtubule affinity regulating kinase 2 signaling cascade mediates calcium-dependent neurite outgrowth. J Neurosci 27:4413–4423.

Uezu A, Fukunaga K, Kasahara J, Miyamoto E (2002) Activation of Ca^{2+}/calmodulin-dependent protein kinase I in cultured rat hippocampal neurons. J Neurochem 82:585–593.

Wang CL, Zhang L, Zhou Y, Zhou J, Yang XJ, Duan SM, Xiong ZQ, Ding YQ (2007) Activity-dependent development of callosal projections in the somatosensory cortex. J Neurosci 27:11334–11342.

Wang DD, Kriegstein AR (2008) GABA regulates excitatory synapse formation in the neocortex via NMDA receptor activation. J Neurosci 28:5547–5558.

Wayman GA, Kaech S, Grant WF, Davare M, Impey S, Tokumitsu H, Nozaki N, Banker G, Soderling TR (2004) Regulation of axonal extension and growth cone motility by calmodulin-dependent protein kinase I. J Neurosci 24:3786–3794.

Wayman GA, Impey S, Marks D, Saneyoshi T, Grant WF, Derkach V, Soderling TR (2006) Activity-dependent dendritic arborization mediated by CaM-kinase I activation and enhanced CREB-dependent transcription of Wnt-2. Neuron 50:897–909.

Yokokura H, Terada O, Naito Y, Hidaka H (1997) Isolation and comparison of rat cDNAs encoding Ca^{2+}/calmodulin-dependent protein kinase I isoforms. Biochim Biophys Acta 1338:8–12.

Supplemental Figures for Ageta-Ishihara et al.

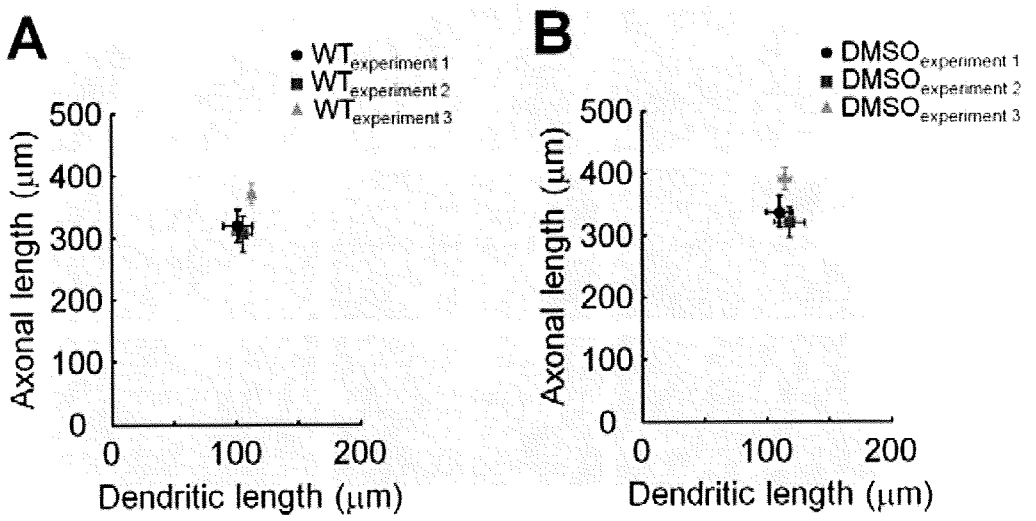

Supplemental Fig. 1. Orthogonal plotting of axonal and dendritic lengths reveals a high degree of consistency across distinct sets of experiments in either mouse or rat cortical neurons.

(A) The panel shows a quantitative analysis of axonal and dendritic morphometric parameters from cultured cortical neurons generated from wild-type (WT) mice brains in three separate sets of experiments. Number of neurons: experiment 1, n = 15; experiment 2, n = 17; experiment 3, n = 20.

(B) The panel shows a quantitative analysis of axonal and dendritic lengths from cultured rat cortical neurons treated with DMSO in three separate sets of experiments. Number of neurons: experiment 1, n = 15; experiment 2, n = 18; experiment 3, n = 15.

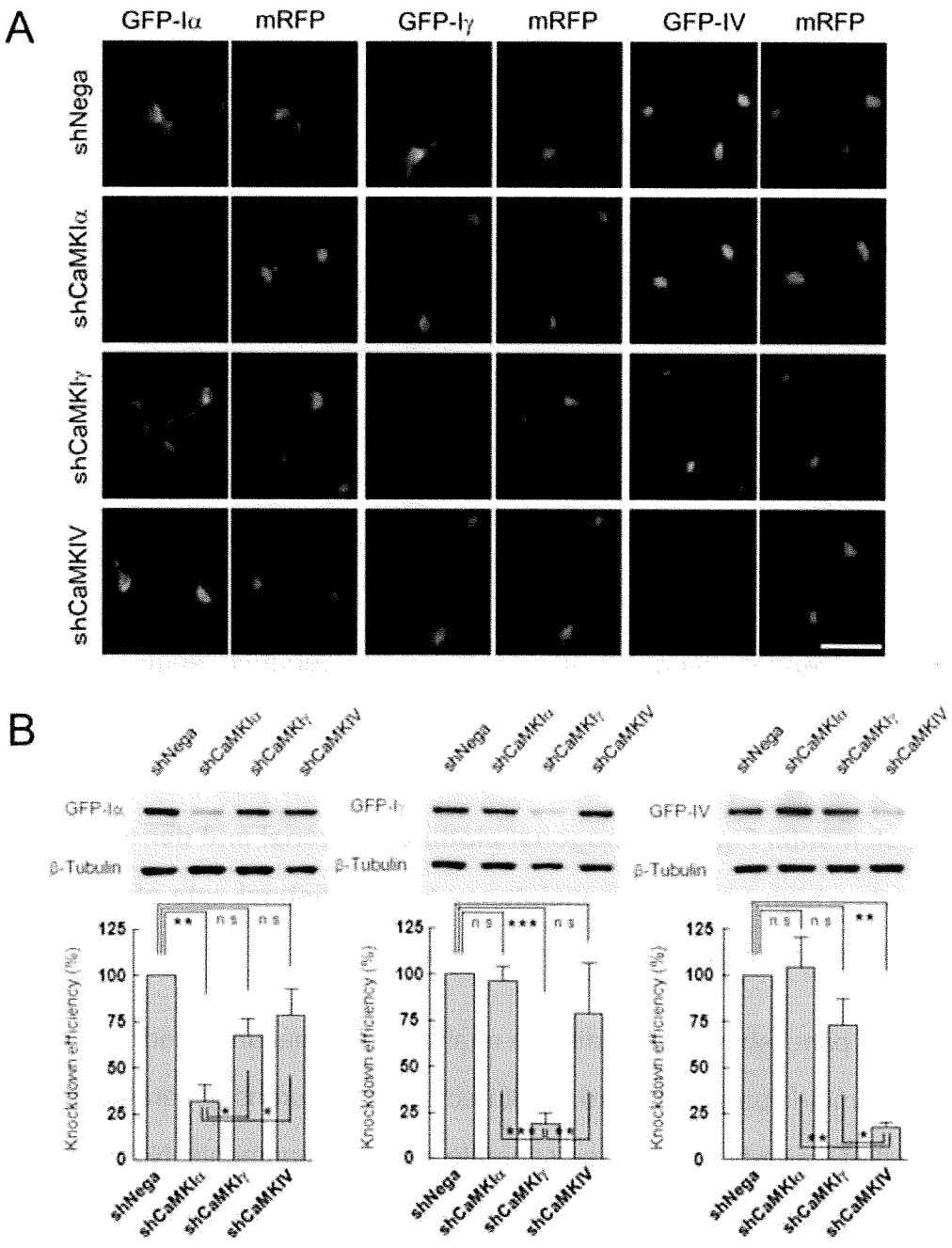
A
GFP-Iα
mRFP
GFP-Iγ
mRFP
GFP-IV
mRFP
shNega
shCaMKIα
shCaMKIγ
shCaMKIV
B
shNega
shCaMKIα
shCaMKIγ
shCaMKIV
GFP-Iα
β-Tubulin
GFP-Iγ
β-Tubulin
GFP-IV
β-Tubulin
Knockdown efficiency (%)
125
100
75
50
25
0
**
ns
ns
***
ns
ns
ns
**
C
relative transcript (a.u.)
1.25
1.00
0.75
0.50
0.25
0.00
***
*
**
shNega
shCaMKIα
shCaMKIγ
shCaMKIV
Camk1a
Camk1g
Camk4

2

Supplemental Fig. 2. Lack of cross-knockdown effects between shCaMKIα, shCaMKIγ, and shCaMKIV.

(A). Single-cell immunocytochemical quantification of knockdown effects. Efficient downregulation of exogenous GFP-CaMKIα was achieved by a CaMKIα-targeted shRNA vector (shCaMKIα), but not by a control vector (shNega), a CaMKIγ/CL3-targeted shRNA vector (shCaMKIγ), or a CaMKIV-targeted shRNA vector (shCaMKIV) in rat cortical neurons. The mRFP1 expression, which was driven by a dual promoter in a pSUPER+mRFP1 vector, remained unchanged. Similarly, efficient downregulation of exogenous GFP-CaMKIγ/CL3 was achieved by shCaMKIγ, but not by shNega, shCaMKIα, or shCaMKIV. Efficient downregulation of exogenous GFP-CaMKIV was achieved by shCaMKIV, but not by shNega, shCaMKIα, or shCaMKIγ. Bar, 50 μm.

(B). Same experiments as (A), except that Western blot analyses against the GFP-tag (with β-tubulin as a control) was performed to quantify the shRNA-dependent suppression. For each experiment, the signal ratio between GFP and β-tubulin immunoreactivities in the shNega samples were considered as 100%, and all data were normalized accordingly. N=3; *, $p< 0.05$; **, $p<0.01$; ***, $p< 0.001$; n.s., not significant ($p> 0.05$) (one-way ANONA followed by post hoc Tukey-Kramer test).

(C) Quantitative real-time PCR analysis of shNega-, shCaMKIα-, shCaMKIγ-, shCaMKIV-electroporated cortical neurons revealed a target-specific decrease of 40~50% in the amount of endogenous mRNA for CaMKIα, CaMKIγ, or CaMKIV, respectively. N=3; *, $p< 0.05$; **, $p<0.01$; ***, $p< 0.001$ (ANONA followed by post hoc Tukey test).

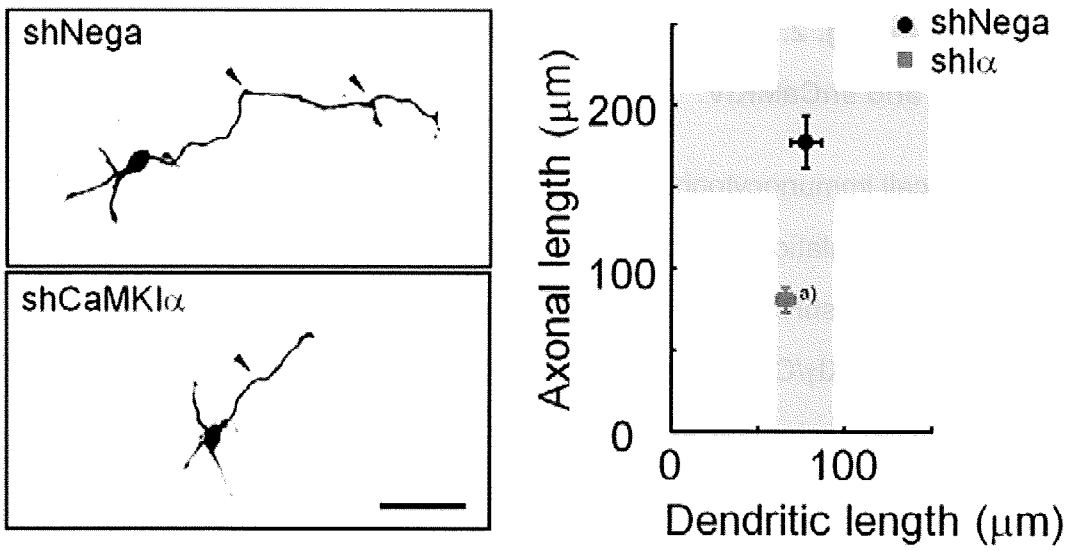

Supplemental Fig. 3. Maximized CaMKIα-knockdown at the time of initial plating results in specific axonal growth impairment while sparing dendrite growth.

Maximal knockdown was achieved by performing a 2-day long suspension culture of transfected cortical neurons prior to re-trituration and plating. shCaMKIα-expressing neurons showed a specific impairment of axonal growth (arrowheads). n = 15 for all groups. [a)] Axon, $p<0.001$ (Student t-test comparison with shNega). Scale bar, 50 μm.

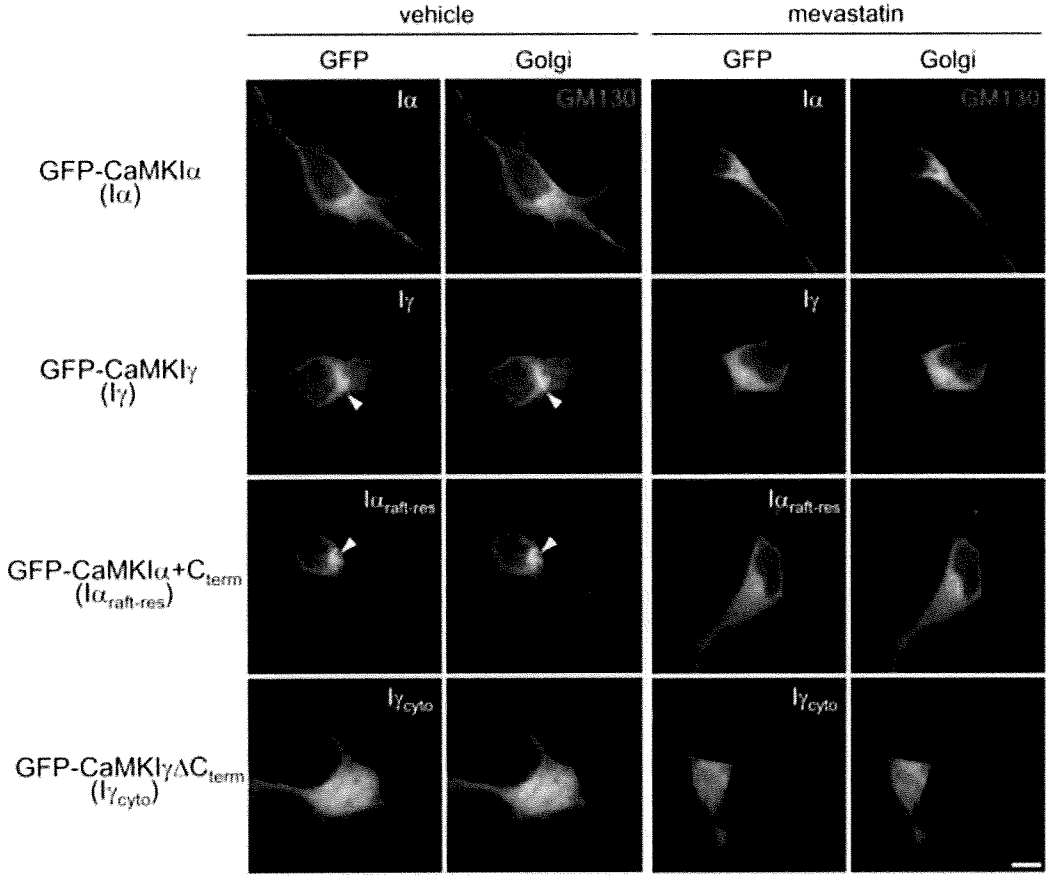

Supplemental Fig. 4.

Lipid modification in the C-terminus of CaMKIγ and CaMKIα+C_{term} ($Iα_{raft-res}$) is critical for Golgi localization.

The subcellular localization of CaMKIα (Iα), CaMKIγ/CL3 (Iγ) and their chimeras in the absence or presence of 10 μM mevastatin, an HMG-CoA reductase inhibitor. Both GFP-Iγ and -$Iα_{raft-res}$ signals were highly colocalized with the Golgi marker GM130 (arrowheads) in the absence of mevastatin. However, these signals became diffuse after mevastatin treatment, confirming the critical role of C-terminal lipid modification of Iγ in Golgi membrane insertion. Bar, 5 μm.

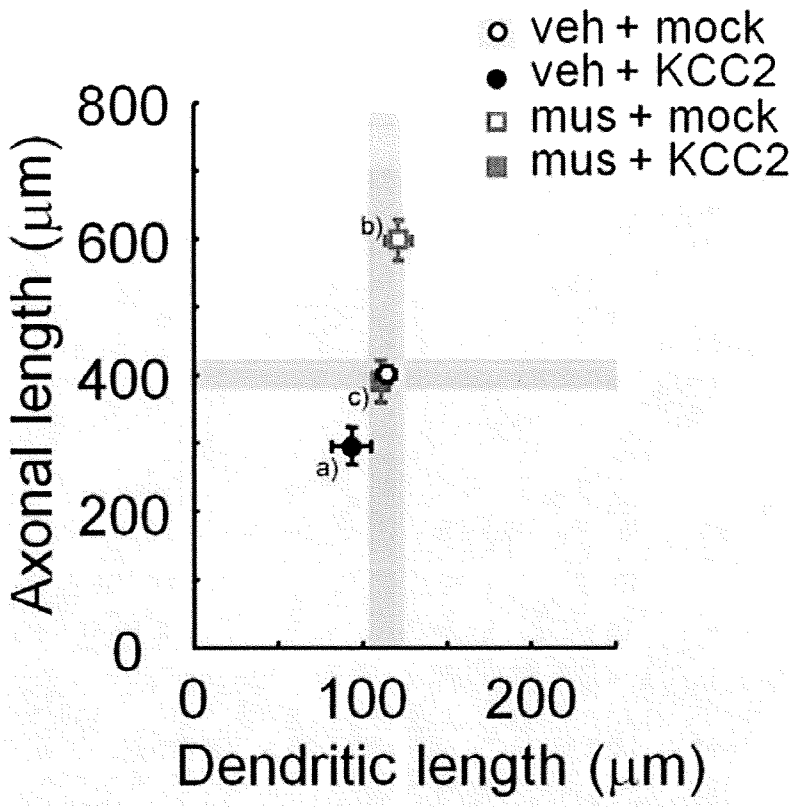

Supplemental Fig. 5. Forced expression of KCC2, a neuronal K^+/Cl^- co-transporter, impaired both constitutive and muscimol-stimulated axonal growth.

n = 15 for all groups. (Axon: two-way ANOVA, muscimol effect, $F_{1,56} = 31.58$, $p<0.0001$; KCC2 effect, $F_{1,56} = 37.15$, $p<0.0001$; muscimol x KCC2, $F_{1,56} = 4.05$, $p = 0.0491$). (Dendrite: two-way ANOVA, muscimol effect, $F_{1,56} = 2.25$, $p = 0.1393$; KCC2 effect, $F_{1,56} = 3.84$, $p = 0.0549$; muscimol x KCC2, $F_{1,56} = 0.43$, $p = 0.5144$). [a), b)] Axon, $p<0.001$ (comparison with vehicle + mock), [c)] Axon, $p<0.001$ (comparison with muscimol + mock), $p<0.05$ (comparison with vehicle + KCC2).

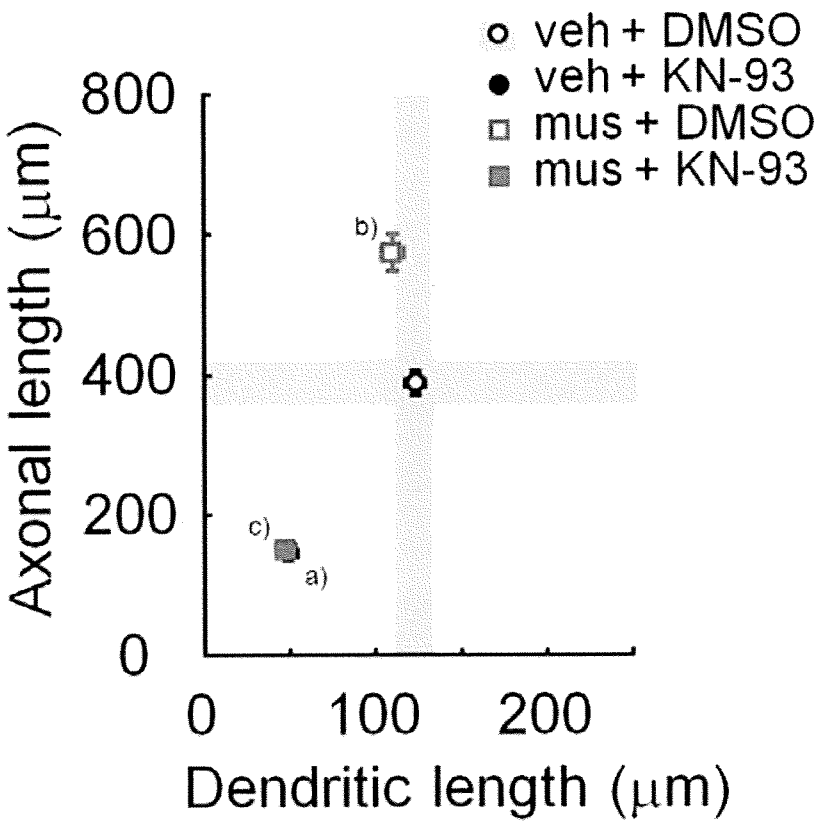

Supplemental Fig. 6. A general CaMK inhibitor KN-93 potently blocked both basal and muscimol-stimulated axonal growth.

Cortical neurons were treated with muscimol from 6 h to 48 h after plating, in the presence or absence of KN-93, a general CaM kinase inhibitor. Muscimol-stimulated axonal growth was strongly suppressed with KN-93. n = 15 for all groups. (Axon: two-way ANOVA, muscimol effect, $F_{1,56} = 30.96$, $p<0.0001$; drug effect, $F_{1,56} = 365.51$, $p<0.0001$; muscimol x drug, $F_{1,56} = 26.33$, $p<0.0001$). (Dendrite: two-way ANOVA, muscimol effect, $F_{1,56} = 1.53$, $p = 0.2206$; drug effect, $F_{1,56} = 131.24$, $p<0.0001$; muscimol x drug, $F_{1,56} = 0.93$, $p = 0.3391$). [a), b)] Axon, $p<0.001$ (comparison with vehicle + DMSO), [c)] Axon, $p<0.001$ (comparison with muscimol + DMSO), n.s. (comparison with vehicle + KN-93) .

nature Vol 465|13 May 2010|doi:10.1038/nature09033

ARTICLES

Widespread transcription at neuronal activity-regulated enhancers

Tae-Kyung Kim[1]*†, Martin Hemberg[2]*, Jesse M. Gray[1]*, Allen M. Costa[1], Daniel M. Bear[1], Jing Wu[3], David A. Harmin[1,4], Mike Laptewicz[1], Kellie Barbara-Haley[5], Scott Kuersten[6], Eirene Markenscoff-Papadimitriou[1]†, Dietmar Kuhl[7], Haruhiko Bito[8], Paul F. Worley[3], Gabriel Kreiman[2] & Michael E. Greenberg[1]

We used genome-wide sequencing methods to study stimulus-dependent enhancer function in mouse cortical neurons. We identified ~12,000 neuronal activity-regulated enhancers that are bound by the general transcriptional co-activator CBP in an activity-dependent manner. A function of CBP at enhancers may be to recruit RNA polymerase II (RNAPII), as we also observed activity-regulated RNAPII binding to thousands of enhancers. Notably, RNAPII at enhancers transcribes bi-directionally a novel class of enhancer RNAs (eRNAs) within enhancer domains defined by the presence of histone H3 monomethylated at lysine 4. The level of eRNA expression at neuronal enhancers positively correlates with the level of messenger RNA synthesis at nearby genes, suggesting that eRNA synthesis occurs specifically at enhancers that are actively engaged in promoting mRNA synthesis. These findings reveal that a widespread mechanism of enhancer activation involves RNAPII binding and eRNA synthesis.

During development and in mature organisms, cells respond to changes in their environment in part through changes in gene expression. Extracellular factors including growth factors, hormones and neurotransmitters activate programs of new gene expression in a manner that is temporally and spatially controlled by the coordinated action of *trans*-acting transcription factors that bind to *cis*-acting DNA regulatory elements including enhancers, insulators and promoters. Most studies of the mechanisms by which gene expression is induced in response to extracellular stimuli have focused on promoters, which lie adjacent to the site at which mRNA synthesis is initiated. In contrast, the mechanisms by which enhancers[1], which lie far away from the start site of mRNA synthesis, contribute to stimulus-dependent gene expression are not well characterized. In the nervous system, hundreds of genes are induced in response to sensory experience-dependent neuronal activation[2]. Exposure of primary neuronal cultures to an elevated level of potassium chloride (KCl) leads to membrane depolarization and an influx of calcium through L-type voltage-sensitive calcium channels[2]. The resulting increase in intracellular calcium level then triggers several calcium-dependent signalling pathways that ultimately lead to changes in gene expression. We used this *in vitro* neuronal culture system to characterize neuronal activity-regulated enhancers.

Defining activity-regulated enhancers

Recent genome-wide studies have established that enhancers can be defined as DNA sequences that bind the transcriptional co-activator p300/CBP, that bind histone H3 monomethylated at lysine 4 (H3K4me1), and that are located distally from known transcription start sites (TSSs)[3–5]. We applied these criteria to define neuronal activity-regulated enhancers. Using ChIP-Seq[6], we first identified CBP binding sites throughout the mouse genome using two different antibodies against CBP and selected only those CBP-bound genomic loci detected by both antibodies (Methods). We found that CBP binding genome-wide is markedly increased upon membrane depolarization (Figs 1, 2, middle, and Supplementary Figs 1e, 2 and 3). Before stimulation, we detected fewer than 1,000 CBP binding sites, whereas upon membrane depolarization we detected ~28,000 CBP binding sites (Methods). Of the CBP sites detected upon membrane depolarization, ~25,000 were at least 1 kilobase (kb) distal to known TSSs, suggesting that most activity-dependent CBP binding does not occur at promoters. To identify specifically CBP binding sites at enhancers, we asked which of the distal CBP sites are also bound by H3K4me1-modified histones, which mark active chromatin regions including enhancers[3,7,8]. About 13,000 distal CBP sites are located within 2 kb of H3K4me1-modified regions (Figs 1, 2b and Supplementary Figs 1c and 3). We removed from this enhancer list a subset (7%) of enhancers that in addition to binding H3K4me1 also bind the transcription-initiation-site-associated histone mark H3K4me3 (refs 7, 8) and therefore may represent uncharacterized promoters (Figs 1, 2, top, and Supplementary Figs 1c, 3 and 8a). We defined the remaining ~12,000 genomic loci where distal CBP sites are flanked by H3K4me1 as neuronal enhancers (see Methods for detailed description of enhancer definition). Approximately half of the neuronal enhancers have evolutionarily conserved sequences in the region of CBP binding, indicating that these enhancers are functionally important (Fig. 1 and Supplementary Fig. 1a, b).

The strong inducibility of CBP binding at thousands of neuronal enhancers and their presence near activity-regulated genes (for

[1]Department of Neurobiology, Harvard Medical School, 220 Longwood Avenue, Boston, Massachusetts 02115, USA. [2]Department of Ophthalmology, Children's Hospital Boston, Center for Brain Science and Swartz Center for Theoretical Neuroscience, Harvard University, 300 Longwood Avenue, Boston, Massachusetts 02115, USA. [3]The Solomon H. Snyder Department of Neuroscience, Johns Hopkins University School of Medicine, 725 North Wolfe Street, Baltimore, Maryland 21205, USA. [4]Children's Hospital Informatics Program at the Harvard-MIT Division of Health Sciences and Technology, 300 Longwood Avenue, Boston, Massachusetts 02115, USA. [5]Molecular Genetics Core facility, Children's Hospital Boston, 300 Longwood Avenue, Boston, Massachusetts 02115, USA. [6]Epicentre Biotechnologies, 726 Post Road, Madison, Wisconsin 53713, USA. [7]Institute for Molecular and Cellular Cognition (IMCC), Center for Molecular Neurobiology (ZMNH), University Medical Center Hamburg-Eppendorf (UKE), Falkenried 94, 20251 Hamburg, Germany. [8]Department of Neurochemistry, Graduate School of Medicine, University of Tokyo, Bunkyo-ku, Tokyo 113-0033, Japan. †Present addresses: University of Texas Southwestern Medical Center, Department of Neuroscience, 5323 Harry Hines Blvd, Dallas, Texas 75390-9111, USA (T.-K.K.); Graduate Program in Neuroscience, University of California San Francisco, 1550 4th Street, San Francisco, California 94158, USA (E.M.-P.).
*These authors contributed equally to this work.

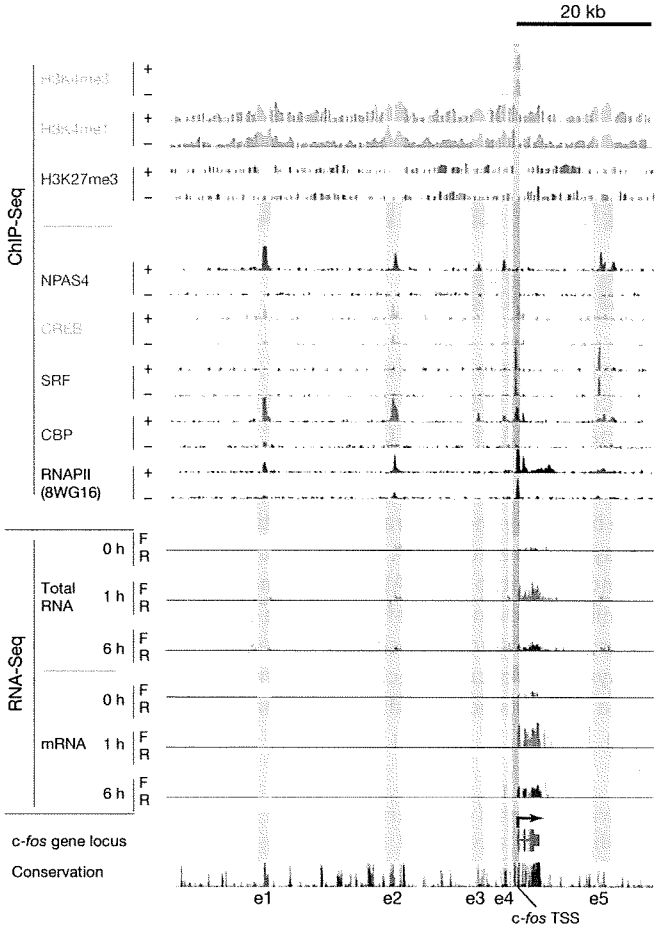

Figure 1 | Enhancers near the c-*fos* gene with increased CBP/RNAPII/NPAS4 binding and eRNA production upon membrane depolarization. ChIP-Seq: for each histone modification or transcription factor, two horizontal rows display the numbers of input-normalized ChIP-Seq reads across the locus, with '+' and '–' denoting the membrane-depolarized (2 h KCl) and unstimulated conditions, respectively. RNA-Seq: for each of 0, 1, or 6 h of membrane depolarization, the numbers of reads aligning to forward (F) and reverse (R) genomic strands are separately displayed. Enhancers identified in this study are highlighted by light-blue vertical bars (e1–e5), and the promoter region of c-*fos* gene is shown by a vertical light-red bar.

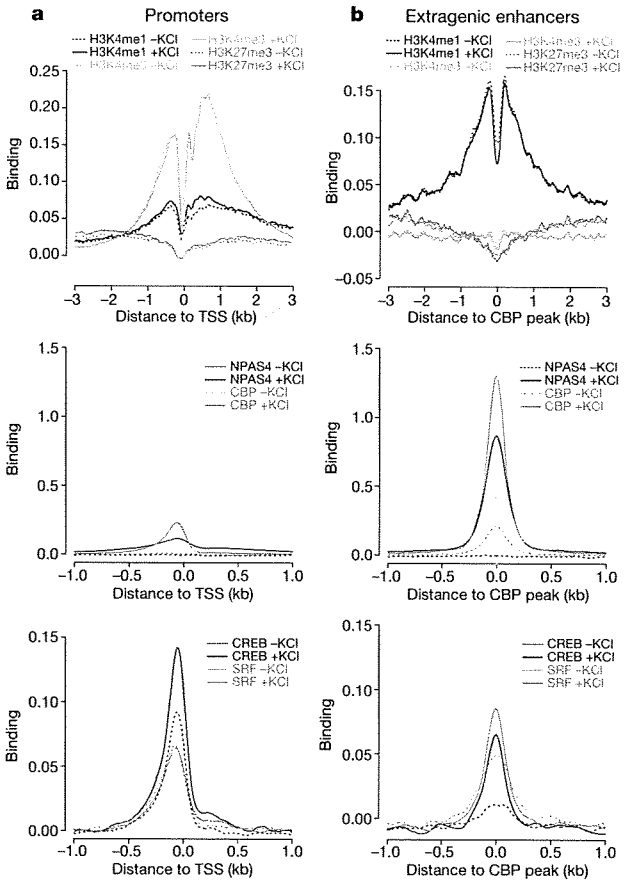

Figure 2 | Comparison of binding profiles between promoters and neuronal activity-regulated enhancers. a, b, Binding profiles of methylated histones and transcription factors at the promoter transcription start sites (TSSs) of 25,562 annotated genes (**a**) versus 5,117 extragenic enhancers (**b**). In each panel, binding profiles of methylated histones (top), CBP and NPAS4 (middle), and CREB and SRF (bottom) from unstimulated and membrane-depolarized (2 h KCl) neurons are shown. The *y* axes denote the degree of binding averaged across all promoters or enhancers, expressed as the mean number of input-normalized ChIP-Seq reads. Promoters are aligned at their annotated TSSs and enhancers are aligned at their CBP binding sites, with the *x* axes indicating the distance (kb) to either the TSS or the CBP peak.

example, c-*fos*, *Rgs2* and *Nr4a2*) (Figs 1, 2b, middle, and Supplementary Table 2) indicate that these enhancers may contribute to the induction of activity-regulated gene expression. One activity-regulated neuronal enhancer was independently identified as an enhancer that drives the activity-regulated transcription of *Arc* (also called *arg3.1*), a gene that regulates synaptic function[9–12]. This *Arc* enhancer, which is located 7 kb upstream of the *Arc* TSS, is necessary to drive activity-regulated *Arc* transcription[13,14]. To determine if the activity-regulated enhancers we identified have the ability to induce transcription at a promoter in an activity-dependent manner, we tested seven of the enhancers in a luciferase reporter assay (Fig. 3). We found that six out of seven enhancers were able to induce expression of luciferase in an activity-dependent manner. Consistent with the known properties of enhancers, the induction of luciferase expression required the presence of an intact promoter.

Characterization of enhancers

We next asked what properties of the enhancers in addition to CBP binding change dynamically when neurons are exposed to a stimulus that triggers activity-regulated gene transcription. H3K4me1 shows a bi-modal pattern of binding that spans a 2–4-kb region with CBP binding at its centre. We defined these H3K4me1-binding regions[60] surrounding CBP binding sites as enhancer domains (Fig. 2b, top, and Supplementary Fig. 1c). The enhancer domains have very low levels of H3K4me3 and are devoid of H3K27me3, a histone marker that has been shown to be associated with either repressed or inactive genes (Fig. 2b, top). Furthermore, the levels of these histone marks are not significantly changed with membrane depolarization, suggesting that enhancer domains are maintained in an open chromatin conformation that is accessible for transcription factor binding, even in the absence of gene induction.

We asked whether transcription factors that are known to mediate activity-regulated gene expression bind to enhancers constitutively or in an activity-regulated manner. CREB, SRF and NPAS4 are known activity-regulated transcription factors that have an important role in various aspects of brain development including neuronal survival, synapse development and synaptic plasticity[15,16]. We find in neurons that CREB, SRF and NPAS4 bind to neuronal enhancers as well as promoters (Supplementary Table 3). Although both CREB and SRF bind enhancers before membrane depolarization, their binding at enhancers in some cases seems to be increased upon membrane depolarization (Fig. 2, bottom, and Supplementary Figs 1d, 2, 4a and 5). In contrast, the binding of NPAS4, which is not present in neurons at significant levels before membrane depolarization[16], was not detected before stimulation but was found at ~28,000

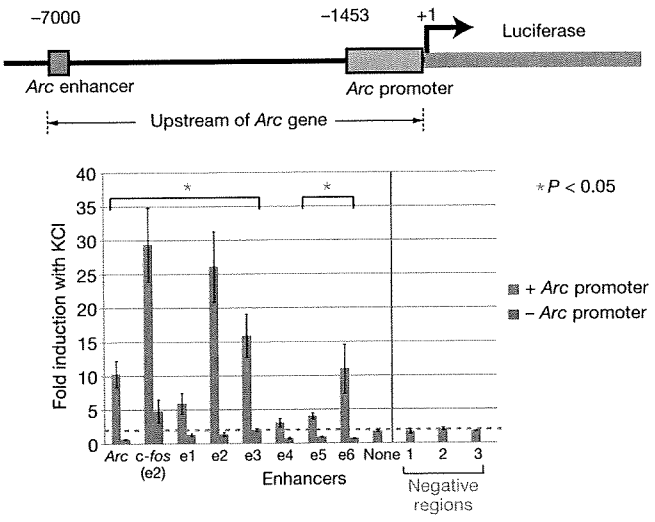

Figure 3 | Activity-induced luciferase expression mediated by neuronal enhancers. The *Arc* enhancer was replaced by six randomly chosen neuronal enhancers and one of the *c-fos* enhancers (e2; see Fig. 1) in the context of the ~7-kb region upstream of the *Arc* gene. The resulting fragments were placed upstream of a luciferase reporter gene, and activity-dependent expression of luciferase was measured in the presence or absence of the *Arc* proximal promoter after 6 h KCl treatment in rat cortical neurons. In additional control experiments, the *Arc* enhancer was removed, or three randomly chosen extragenic loci that do not show enhancer features were inserted. The red dotted line indicates the mean induction value of the three negative regions tested. Error bars indicate s.e.m. ($n = 3$ biological replicates); *P*-value from *t*-test.

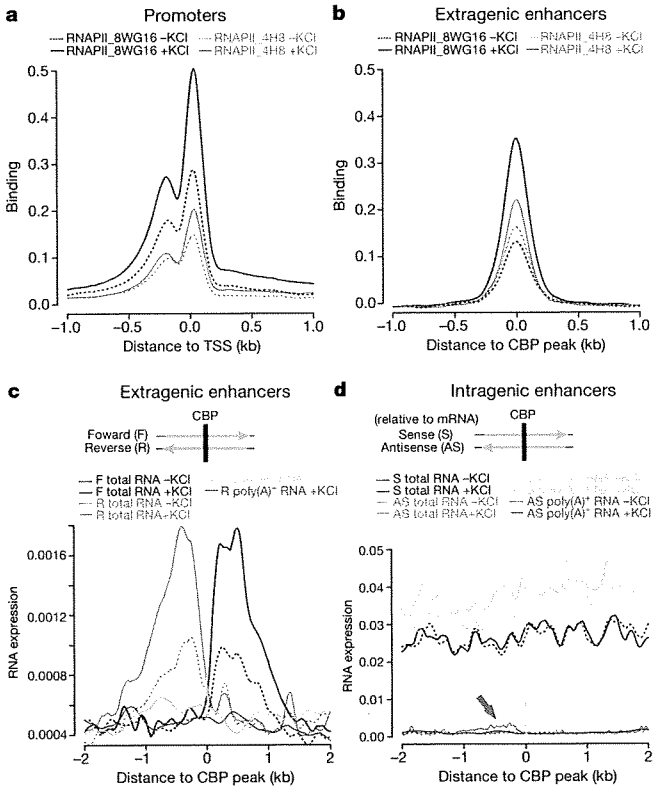

Figure 4 | Enhancers bind RNA polymerase II (RNAPII) and produce eRNAs. **a**, Binding profile of RNAPII at 25,562 TSSs of annotated genes using two different anti-RNAPII antibodies (8WG16 or 4H8). **b**, Binding profile of RNAPII at 5,117 extragenic enhancers. **c**, **d**, Profile of RNA expression at 5,117 extragenic enhancers (**c**) and at 6,718 intragenic enhancers (**d**) based on RNA sequencing of the total RNA and poly(A)$^+$ RNA fractions. The *y* axes report RNA expression as the normalized number of RNA-Seq reads per bp (Methods). In **c**, F and R denote forward (+) and reverse (−) genomic strands. In **d**, enhancers are aligned oriented relative to the gene in which they reside to allow for sense and antisense RNA-Seq reads to be shown separately. Although sense eRNAs cannot be detected due to overlapping mRNA transcription, the red arrow indicates a local increase in antisense RNA expression attributable to eRNAs (statistics in Methods). Note different scales on the *y* axis in **c** and **d**.

sites in membrane-depolarized neurons (Figs 1, 2, middle, and Supplementary Figs 1e, 2 and 3). NPAS4 binding was strongly biased towards enhancers relative to promoters, suggesting that NPAS4 may have a specific role in enhancer function (Supplementary Fig. 4a). Although we have shown that enhancer domains can be as long as 4 kb, our analysis of CREB, SRF, NPAS4 and CBP binding to enhancers indicates that these factors are predominantly located within 100 bp of the highly conserved centre of the enhancer domain (Supplementary Fig. 4b). This tight co-localization of individual transcription factors with CBP at a subset of enhancers (Supplementary Table 4) suggests that transcription factors may work together to regulate enhancer function, possibly by recruiting CBP.

Transcription at enhancers

At promoters, CBP recruits components of the basal transcription machinery, including RNAPII, thereby facilitating the assembly of functional transcription complexes that initiate mRNA synthesis[17]. Because CBP binds to enhancers in an activity-dependent manner, we asked if CBP also recruits RNAPII to these enhancers. To address this issue, we used ChIP-Seq to identify RNAPII binding sites across the genome using two different RNAPII antibodies. Consistent with previous studies[18,19], a large number of RNAPII sites were found to be located near annotated TSSs (Figs 1, 4a and Supplementary Fig. 4a). Notably, RNAPII also bound to ~3,000 activity-regulated enhancers (25%) (Figs 1, 4b and Supplementary Figs 1f, 3 and 4a), and the level of RNAPII binding was increased about twofold upon membrane depolarization (Fig. 4b and Supplementary Fig. 2). Although RNAPII has previously been reported to be present at several enhancers, including the β-globin and MHC class II gene enhancers[20,21], it has not been thought to have a widespread role in enhancer function. Given that CBP was previously known to recruit RNAPII to promoters and that increases in CBP and RNAPII binding coincide at thousands of enhancers in membrane depolarized neurons, it is likely that CBP has a role in the activity-regulated increase in RNAPII binding at enhancers. However, the observation that RNAPII is present at only a subset of CBP-bound enhancers suggests that additional activation steps beyond CBP binding may be required for RNAPII recruitment to enhancers.

The presence of RNAPII at enhancers raises the possibility that RNA transcription may occur at enhancers. Alternatively, the detection of RNAPII at enhancers might be an indirect consequence of the interaction of enhancers with active promoters, such that promoter-bound RNAPII gets crosslinked to enhancer DNA during the preparation of cells for ChIP-Seq experiments. To distinguish between these two possibilities, we used high-throughput RNA sequencing (RNA-Seq) to determine whether enhancer-bound RNAPII drives RNA synthesis at enhancers. Because it was not clear whether enhancer-derived transcripts would be polyadenylated, we sequenced total RNA, obtained from unstimulated or membrane-depolarized neurons after ribosomal RNA was depleted. To distinguish possible enhancer-derived transcripts from mRNA transcripts, we sought evidence of RNA transcription specifically at those ~5,000 activity-regulated enhancers located outside of annotated genes (extragenic enhancers). Surprisingly, we detected short (<2 kb) RNAs at ~2,000 extragenic enhancers (Figs 1, 4c, 5a, c and 6a). We observed dynamic changes in the levels of these enhancer RNAs (eRNAs) upon membrane depolarization, with a mean increase of ~2-fold (Fig. 4c). Synthesis of eRNAs seems to initiate near enhancer centres where CBP and RNAPII are bound and to proceed bi-directionally, extending to the

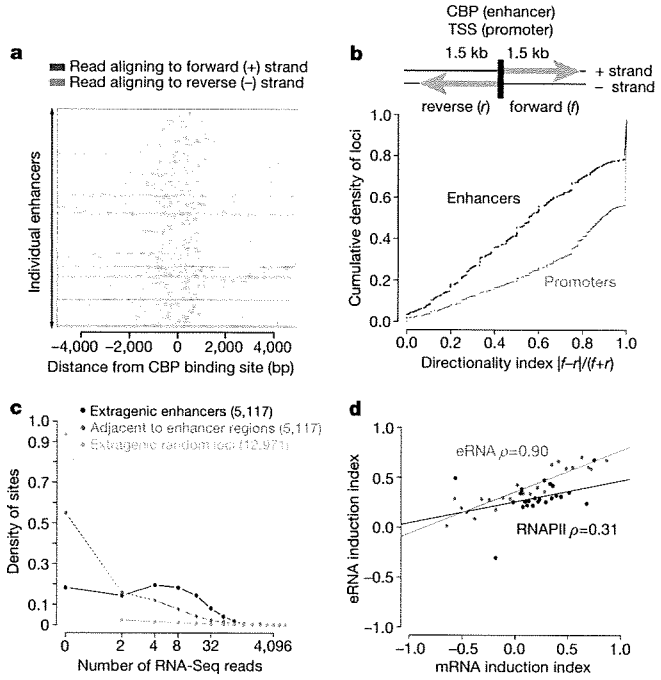

Figure 5 | eRNAs are transcribed bi-directionally, and their activity-dependent induction correlates with induction of nearby genes. **a**, RNA expression at 315 representative extragenic enhancers (see Methods for the enhancer selection and clustering). The enhancers are grouped into six categories using *k*-means clustering based on eRNA, RNAPII, CBP, NPAS4, CREB, SRF and H3K4me1 levels, with categories separated by horizontal black lines[3]. **b**, Directional bias of transcription initiated from enhancers and promoters, where *f* and *r* represent the numbers of reads (forward and reverse, respectively) aligning to the regions indicated (see Methods). **c**, The distribution of the number of RNA-Seq reads found within 1.5 kb of the extragenic enhancer loci, adjacent regions and random regions (see Methods). **d**, Changes in RNAPII binding and eRNA levels at extragenic enhancers versus changes in mRNA expression levels of nearby genes upon membrane depolarization. Each dot represents a set of genes that have similar mRNA induction indices and a corresponding set of enhancers nearby those genes (see Methods). The lines are the best linear fits to the points, and ρ is the Spearman correlation coefficient.

ends of the H3K4me1-modified enhancer domain (Figs 1, 4c, 5a, b, 6a and Supplementary Fig. 7a, b). Interestingly, we also detected eRNAs at ~1,000 of ~7,000 intragenic enhancers (Methods). Although high levels of mRNA transcription across intragenic enhancers prevented accurate quantification of eRNAs in the sense orientation, antisense eRNAs at intragenic enhancers were detectable and were similar in level to eRNAs at extragenic enhancers (Fig. 4c, d and Methods). These observations indicate that enhancers are not only sites where transcription factors bind and recruit RNAPII that might subsequently be delivered to promoters, but that enhancers are also sites where RNA synthesis occurs.

The strand-specific synthesis of eRNAs (Fig. 5a) and the dynamic changes in the level of eRNAs in response to neuronal activity suggest that the detection of eRNAs is not due to the sequencing of residual genomic DNA that is present in our purified RNA samples. Nevertheless, to confirm the existence of activity-regulated eRNAs at enhancers, we used an alternative method (DNaseI treatment followed by quantitative polymerase chain reaction with reverse transcription (RT–qPCR)) to detect these RNA transcripts (Supplementary Fig. 6). By RT–qPCR, we detected eRNAs at each of 18 enhancer loci tested. This result provides independent confirmation that the thousands of distinct eRNAs detected by RNA-Seq are bona fide RNA transcripts that are induced in an activity-dependent manner from neuronal enhancers.

We did not detect eRNAs in RNA-Seq from poly(A)$^+$ RNA fractions, suggesting that a large number of eRNAs may not be polyadenylated.[62] Although it is possible that some polyadenylated eRNAs are present but not detectable at our current sequencing depth, two independent lines of evidence suggest that a large number of eRNAs may not be polyadenylated. First, using RT–qPCR, we observed that eRNAs were detected at higher levels in randomly primed reactions compared to oligo-dT-primed RT reactions (data not shown). Second, conventional sequencing of a circularized eRNA from the *Arc* enhancer confirmed that this transcript is not polyadenylated (Fig. 6). These experiments suggest that polyadenylation may not be a common feature of eRNA synthesis.

The detection of RNAPII binding and RNA synthesis at many enhancers could, in principle, result from mis-categorization of un-annotated promoters as enhancers. However, several lines of evidence suggest that both the extragenic and intragenic enhancers we have identified are indeed enhancers and are not un-annotated promoters. First, histone modification profiles at enhancers and annotated promoters are clearly distinguishable (Fig. 2, top, and Supplementary Figs 1c and 8a). Activity-regulated enhancers have high H3K4me1 and relatively low H3K4me3 levels, whereas promoters have lower H3K4me1 and high H3K4me3 levels. Second, the observation that eRNAs do not extend beyond the ~4-kb enhancer domain suggests that the eRNAs are much shorter (<2 kb for each strand) than transcripts initiated at most gene promoters (Figs 4c and 5a). Third, unlike promoters, enhancers do not produce detectable levels of polyadenylated RNA (Fig. 4c, d). Fourth, a promoter prediction algorithm (ProSOM)[22] revealed that fewer than 100 of ~12,000 enhancer regions are predicted to be promoters compared to 8,494 out of 27,854 annotated TSSs. Fifth, whereas sense transcription is more prevalent than antisense transcription at most promoters, transcription at enhancers seems to be less biased towards one particular strand (Fig. 5b). Finally, a few enhancers, including the well-characterized β-globin enhancer, have previously been shown to recruit RNAPII and drive transcription[23,24]. These findings argue against the possibility that RNAPII-bound enhancers that produce eRNAs are actually un-annotated promoters.

Mechanism of eRNA synthesis

Our observation that only a subset of the ~12,000 enhancers that inducibly bind CBP also bind RNAPII and drive eRNA transcription led us to hypothesize that RNAPII and/or eRNA synthesis might occur at a subset of enhancers that are actively engaged in promoting mRNA synthesis. To test this hypothesis, we investigated whether activity-regulated changes in RNAPII or eRNA levels at enhancers correlate with changes in mRNA levels at nearby genes (Fig. 5d and Supplementary Fig. 7c). The assumption in this analysis is that an enhancer is most likely to promote mRNA synthesis of the nearest gene[3,25]. We found that changes in eRNA expression levels that occur at enhancers upon membrane depolarization are strongly correlated with changes in mRNA expression levels at nearby genes. Changes in RNAPII levels at enhancers are also, to a lesser degree, correlated with changes in mRNA expression levels at nearby genes (Fig. 5d). Given that only a fraction of enhancers show inducible RNAPII binding or inducible eRNA synthesis, the binding of CBP to enhancers may not be sufficient for enhancer activation. Instead, enhancers exhibiting RNAPII binding and eRNA synthesis may represent a subset of CBP-bound enhancers that are actively engaged in promoting mRNA transcription.

The correlation between eRNA and mRNA induction suggests that eRNA synthesis may only occur when an enhancer interacts with the promoter of its target gene. In this scenario, eRNAs should not be generated from an enhancer when its target promoter is absent. We tested this hypothesis in the specific case of the mouse *Arc* enhancer using *Arc* knockout neurons in which most of the *Arc* gene, including the *Arc* promoter, is deleted but the *Arc* enhancer remains intact[10]. To characterize the *Arc* enhancer in *Arc* knockout neurons, we first performed chromatin immunoprecipitation (ChIP) experiments testing for the binding of SRF and RNAPII, two factors that we found